Spin dynamics of chromium. I. Formalism and commensurate alloys

R. S. Fishman
*Solid State Division, Oak Ridge National Lab, Oak Ridge, Tennessee 37831-6032**
and Department of Physics, North Dakota State University, Fargo, North Dakota 58105-5566

S. H. Liu
Department of Physics, University of California, San Diego, California 92093
(Received 24 January 1996; revised manuscript received 1 May 1996)

The spin dynamics of chromium alloys are produced by the fluctuations about a spin-density wave (SDW) consisting of bound electron-hole pairs. While commensurate (C) alloys have a single SDW with wave vector $G/2=2\pi/a$, incommensurate (I) alloys have two SDW's with wave vectors on either side of $G/2$. Spin fluctuations with frequency ω and wave vector q correspond to possible quasiparticle transitions between the two (C) or three (I) bands of hybridized electron and hole energies with energy change ω and momentum change q. This paper develops the random-phase approximation for the spin dynamics of both C and I alloys. The collective excitations of C alloys consist of a transverse spin-wave (SW) mode with linear dispersion and a longitudinal amplitude mode. Incoherent spin fluctuations lie above the amplitude mode frequency and below the SW frequency. While the SW mode involves the rigid rotation of the local magnetic moments, the amplitude mode involves the oscillation of the SDW amplitude, which decays in time according to a power law. [S0163-1829(96)06834-8]

I. INTRODUCTION

The magnetic and metallic properties of transition-metal antiferromagnets are intimately related. It is well-known[1] that the spin-density wave (SDW) in Cr and γ-Mn alloys is produced by the nearly perfect nesting of electron and hole Fermi surfaces. Unlike the local magnetic moments of rare-earth antiferromagnets, the SDW of itinerant antiferromagnets consists of bound electron-hole pairs. Depending on impurity levels, the periodicity of the SDW in Cr may be either commensurate (C) or incommensurate (I) with the bcc lattice. While the CSDW state has a single wave vector $G/2=2\pi/a$, the ISDW state superimposes two SDW's with wave vectors on either side of $G/2$. Although neutron scattering has provided a wealth of data[2–10] on the dynamical properties of Cr alloys, theoretical work has lagged behind. Previous studies[11–13] of the C spin dynamics were restricted to either zero temperature or perfect nesting. This paper develops the random-phase approximation (RPA) for the spin dynamics of itinerant antiferromagnets, and then applies that formalism to the dynamics of a CSDW state. We describe the spin dynamics of C alloys for arbitrary values of doping and temperature. In the following paper[14] (paper II), we apply the RPA to the spin dynamics of I Cr alloys.

Chromium alloys are prone to the formation of a SDW because of the nearly identical size and octahedral shape of the electron a and hole b Fermi surfaces[1] centered at the Γ and H points in reciprocal space. The wave vectors which nest these Fermi surfaces in Fig. 1 are $Q_{\pm}=2\pi(1\pm\partial)/a$, where ∂ measures the size difference between the Fermi surfaces. For pure Cr, $\partial\approx 0.05$, so the hole surface is only slightly larger than the electron surface. The other structures in Fig. 1 form the ''electron reservoir,'' which is discussed in paper II.

Below the Néel temperature T_N, the Coulomb attraction $U>0$ between the electrons and holes produces a SDW consisting of bound electron-hole pairs in a spin-triplet state with order parameter g. In order to minimize the nesting free energy on both sides of the Fermi surfaces,[15] the actual wave vectors $Q'_{\pm}=2\pi(1\pm\partial')/a$ of the SDW are closer to $G/2$ than the nesting wave vectors $Q_{\pm}$.

Three domains for the SDW wave vectors $\mathbf{Q}'_{\pm}$ correspond to the possible directions of the nesting wave vectors $\mathbf{Q}_{\pm}$. A single domain of the ISDW can be selected by cooling an I alloy below the Néel temperature in a magnetic field $\mathbf{H}$ along

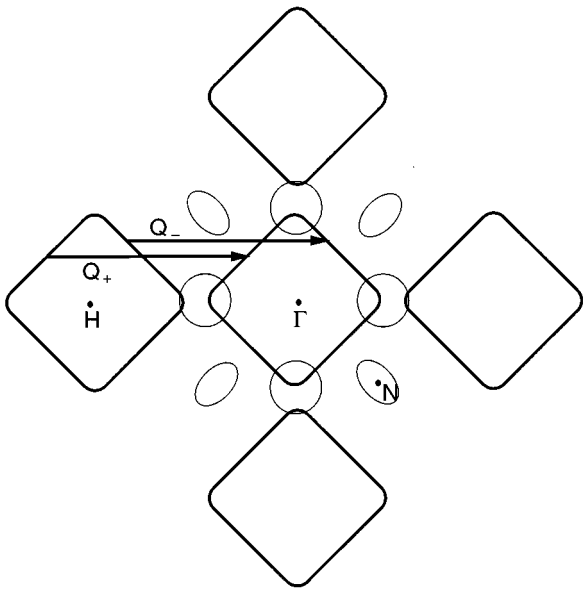

FIG. 1. The hole and electron Fermi surfaces with nesting wave vectors $Q_{\pm}$. Also drawn are other bands which form the ''electron reservoir.''

one of the crystal axes. The SDW wave vectors will then be aligned parallel to **H**. In this paper, we choose the SDW wave vectors to lie along the z direction.

The ''canonical'' free energy F of Cr alloys is constructed by integrating the self-consistent equation for the SDW order parameter g. The SDW wave vectors are then obtained by minimizing[15] F with respect to ∂'. For I alloys, ∂' lies between 0 and ∂. In the C phase, the size mismatch ∂ between the electron and hole Fermi surfaces is sufficiently small that the free energy is minimized when $\partial'=0$ and $Q'_{\pm}=G/2$. The ''canonical'' free energy neglects higher harmonics of the SDW, such as the charge-density wave[16] (CDW) with wave vectors $2Q'_{\pm}$.

Experimentally, ∂ can be controlled through doping: while alloying with Mn or Fe raises the chemical potential μ and decreases the mismatch, alloying with V lowers μ and increases ∂. For $Cr_{1-x}Mn_x$ alloys, the triple point[1] lies at $x\approx 0.003$: for $Cr_{1-x}Fe_x$ alloys, it falls at the higher value of $x\approx 0.02$. Whereas the Néel temperature increases as ∂ decreases and the nesting improves, T_N decreases as ∂ increases and the nesting worsens. In $Cr_{1-x}V_x$ alloys, the Néel temperature vanishes when x exceeds 0.04. Regardless of doping levels, however, electron scattering[15] by phonons and impurities always suppresses both the order parameter and the Néel temperature.

Unlike the local moments of a rare-earth antiferromagnet, which are fixed in magnitude by the spin quantization condition $S^2=\hbar^2 s(s+1)$, the magnetic moments of a transition-metal antiferromagnet can fluctuate in magnitude with the formation and separation of electron-hole pairs. Consequently, the spin dynamics of an itinerant antiferromagnet is much more complex than for a local-moment system. Besides conventional spin-wave (SW) modes, in which the magnetic moments rotate rigidly, the excitation spectrum also contains amplitude modes, in which the magnitudes of the magnetic moments oscillate about their equilibrium values.

The spin dynamics of transition-metal antiferromagnets like Cr are driven by quasiparticle transitions. Spin excitations with frequency ω and wave vector $p=q+G/2$ about a static SDW with wave vector $Q'=w+G/2$ are associated with quasiparticle transitions with energy difference ω and momentum difference $q-w$. So the collective modes depend very sensitively on the quasiparticle energies.

The simplest model for the quasiparticle energies of I alloys is the two-band model first introduced by Fedders and Martin.[11] Since it assumes that each ISDW is generated independently, this model does not allow quasiparticle transitions between the two ISDW states with momenta $Q'_{\pm}$. A more realistic three-band model for the quasiparticle energies was later developed by Young and Sokoloff.[16] Within the three-band model, the nesting on one side of the Fermi surface is directly affected by the mismatch on the other side. Consequently, quasiparticle transitions are allowed from one ISDW state to the other, and the dynamics about one ISDW is intimately coupled with the dynamics about the other.

In the C phase, the dynamics of the two- and three-band models are identical. But due to its complexity, the C dynamics has only been previously solved[11–13] in the limits of zero temperature or perfect nesting with $\partial=0$. The sole Goldstone modes of a CSDW are the transverse SW modes, which are associated with the rotational symmetry of the C free energy about the spin polarization direction $\hat{m}$. We will show that SW's have a linear dispersion $\omega_t=cq$, with a mode velocity $c=v_F/\sqrt{3}$ which is independent of both temperature and wave-vector mismatch ∂.

Because the SDW consists of bound electron-hole pairs, the SW modes in an itinerant antiferromagnet may be quite different than the rigidly rotating spins in a Heisenberg antiferromagnet. Nontheless, SW's in itinerant and local-moment antiferromagnets bear many striking similarities. For example, the susceptibility of SW's about a CSDW has precisely the same functional form as in a Heisenberg antiferromagnet. Since the nonrigid rotation of the spins within a CSDW would cost a nonzero pair-breaking energy, SW's in a CSDW state must also correspond to the rigid rotation of the spin at every lattice site.

A longitudinal mode with frequency ω_l is associated with collective oscillations of the CSDW amplitude above the pair-breaking energy $2\Delta=2\sqrt{2}g$. At $q=0$, the amplitude mode frequency $\omega_l(q)$ has a minimum of 2Δ. For any wave vector, the amplitude mode frequency is always larger than the SW mode frequency $\omega_t(q)$, so the two modes never cross. But unlike the SW mode, the amplitude mode is not associated with a δ function[18] in the susceptibility. Consequently, oscillations of the CSDW amplitude decay according to a power law.

At frequencies above $\omega_l(q)$ or below $\omega_t(q)$, quasiparticle transitions produce an incoherent background of spin excitations. Between $\omega_t(q)$ and $\omega_l(q)$, quasiparticle transitions are prohibited, so the neutron-scattering cross section must vanish. Since $2\Delta(0)\approx 280$ meV, most experiments are performed at frequencies far below the pair-breaking threshold $2\Delta(T)\leqslant\omega_l(q)$. In this regime, SW modes dominate the in-

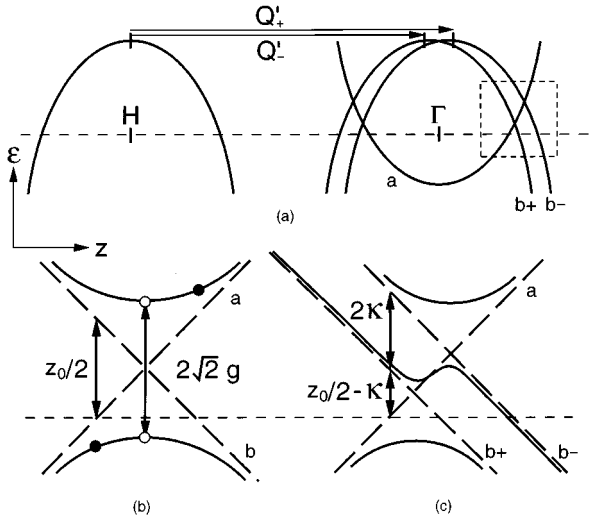

FIG. 2. (a) The unshifted and shifted paramagnetic energies plotted vs $z=v_F(\hat{n}\cdot\mathbf{k}-k_F)$. The region near the Fermi energy is magnified for the (b) C and (c) I ($k_z>0$) phases, with the paramagnetic energies given by the dashed lines and the hybridized energies below the Néel temperature given by the solid curves. For $k_z<0$, the $b+$ and $b-$ labels in (c) would be switched. The chemical potential is denoted by a horizontal dashed line in all three plots. Special C transitions discussed in the text are represented by filled and empty circles.

coherent background and, the dynamical response can be simply approximated by Eq. (40) for the cross section of the SW modes. Only at high frequencies, or close enough to the Néel temperature that $\omega > 2\Delta(T)$, does the incoherent background become important.

The formalism developed in this paper for the C spin dynamics can also be applied to γ-Mn alloys.[19] Due to the very small mismatch ∂ between its electron and hole Fermi surfaces, a γ-Mn alloy is always in a CSDW state. Unlike the linear SW dispersion of C Cr alloys, however, the SW dispersion of γ-Mn alloys has a gap at $q=0$. As discussed in the conclusion, this energy gap may be induced by the strong coupling between a CDW and the tetragonal lattice of γ-Mn.

Our motivation in studying the C spin dynamics is twofold. First, the C dynamics is interesting in its own right, and we are hopeful that many of our predictions will be verified by future experiments. Second, the CSDW state of Cr and γ-Mn alloys provide the simplest example of itinerant antiferromagnetism in three dimensions. Due to the simplicity of the C quasiparticle energies, the RPA susceptibilities can be solved analytically and numerical uncertainties are minimized. Paper II will use many of the insights gained in this work to elucidate the more complex I dynamics, which can only be solved numerically.

This paper is divided into five main sections. Section II describes the basic methodology used in both the C and I regimes. In Sec. III, we apply this formalism to the C phase. Section IV describes our results for the C spin dynamics. Finally, Sec. V contains a discussion and conclusion. Most of the formalism and derivations are relegated to the five appendixes referenced in the text. The I dynamics is discussed in paper II.

II. BASIC METHODOLOGY

The spin dynamics of an itinerant antiferromagnet are driven by quasiparticle transitions. So the quasiparticle energies have a profound influence on the dynamics. Following Young and Sokoloff,[16] we introduce the shifted paramagnetic hole energies

$$\epsilon_{b\pm}(\mathbf{k}) = \epsilon_b(\mathbf{k} - \mathbf{Q}'_{\mp}), \tag{1}$$

which are plotted in Fig. 2(a). Near the Fermi energy, the unshifted and linearized electron energy is given by

$$\epsilon_a(\mathbf{k}) = z(\mathbf{k}), \tag{2}$$

where $z(\mathbf{k}) = v_F(\mathbf{k}\cdot\hat{n} - k_F)$ is measured from an octahedral face of the Fermi surface with normal $\hat{n}$. The shifted and linearized hole energies are

$$\epsilon_{b+}(\mathbf{k}) = \frac{z_0}{2} - \kappa\ \mathrm{sgn}(k_z) - z(\mathbf{k}), \tag{3a}$$

$$\epsilon_{b-}(\mathbf{k}) = \frac{z_0}{2} + \kappa\ \mathrm{sgn}(k_z) - z(\mathbf{k}), \tag{3b}$$

where $z_0 = (v_F/\sqrt{3})4\pi\partial/a$ is the energy mismatch between the electron and hole Fermi surfaces and $\kappa = z_0\partial'/2\partial \geqslant 0$. In the I phase with $\kappa > 0$, the $b+$ surface is better nested for $k_z > 0$, and the $b-$ surface is better nested for $k_z < 0$. In the C phase with $\kappa = 0$, the nested Fermi surfaces are concentric and the two hole energies $\epsilon_{b\pm}(\mathbf{k}) \equiv \epsilon_b(\mathbf{k})$ are identical. So the nesting on both sides of the hole surface is equivalent.

The paramagnetic energies are plotted versus z in the dashed lines of Figs. 2(b) and 2(c). Lying an energy $z_0/4$ below the geometric center of both plots, the chemical potential is denoted by a dashed vertical line. In each plot, the origin $(z,\epsilon) = (0,0)$ lies at the intersection of the chemical potential with the electron energy ϵ_a.

To simplify our calculations, we assume that the wave vector $\mathbf{q}$ of the spin fluctuations is parallel to the wave vectors $\mathbf{Q}'_{\pm} = Q'_{\pm}\hat{z}$ of the SDW. If q is small compared with k_F, then fluctuations remain close to an octahedral face of the Fermi surface and

$$z(\mathbf{k}+\mathbf{q}) = z(\mathbf{k}) + v_F\hat{n}\cdot\mathbf{q} = z(\mathbf{k}) + \xi\ \mathrm{sgn}(k_z), \tag{4}$$

where $\xi \equiv v_F|\mathbf{q}|\mathrm{sgn}(q_z)/\sqrt{3}$. The factor of $\sqrt{3}$ from $|\hat{n}\cdot\hat{z}| = 1/\sqrt{3}$ eventually appears in the SW mode velocity $c = v_F/\sqrt{3}$. With the assumption $q \ll k_F < 2\pi/a$, our results are only valid near the magnetic satellites. But the observed spin excitations also lie close to the magnetic satellites.

In the Heisenberg representation, the second-quantized operators are

$$\underline{\Psi}(\mathbf{k},\tau) = e^{-\tau(\mu N - H)}\underline{\Psi}_{\mathbf{k}}e^{\tau(\mu N - H)}, \tag{5}$$

where

$$\underline{\Psi}_{\mathbf{k}} = \begin{pmatrix} a_{\mathbf{k}\uparrow} \\ a_{\mathbf{k}\downarrow} \\ b^{(-)}_{\mathbf{k}\uparrow} \\ b^{(-)}_{\mathbf{k}\downarrow} \\ b^{(+)}_{\mathbf{k}\uparrow} \\ b^{(+)}_{\mathbf{k}\downarrow} \end{pmatrix} \tag{6}$$

is a six-dimensional vector in band and spin space. While $a^{\dagger}_{\mathbf{k}\sigma}$ and $a_{\mathbf{k}\sigma}$ create and destroy electrons, $b^{(\pm)}_{\mathbf{k}\sigma}$ and $b^{\dagger(\pm)}_{\mathbf{k}\sigma}$ create and destroy holes on the $b\pm$ bands.

The Matsubara Green's function of Cr is a six-dimensional matrix in band and spin space defined by

$$\underline{G}(\mathbf{k}, i\nu_l) = \int_0^{\beta} d\tau\ \underline{G}(\mathbf{k},\tau)e^{i\nu_l\tau}, \tag{7}$$

$$\underline{G}(\mathbf{k},\tau) = -\langle T_\tau\underline{\Psi}(\mathbf{k},\tau)\underline{\Psi}^{\dagger}(\mathbf{k},0)\rangle, \tag{8}$$

where $\nu_l = (2l+1)\pi T$ are the fermion Matsubara frequencies. Neglecting the CDW, the six-dimensional inverse Green's function is

$$\underline{G}^{-1}(\mathbf{k}, i\nu_l) = \begin{pmatrix} [i\nu_l - \epsilon_a(\mathbf{k})]\underline{1} & -ge^{i\phi_-}\hat{m}\cdot\underline{\boldsymbol{\sigma}} & -ge^{i\phi_+}\hat{m}\cdot\underline{\boldsymbol{\sigma}} \\ -ge^{-i\phi_-}\hat{m}\cdot\underline{\boldsymbol{\sigma}} & [i\nu_l - \epsilon_{b-}(k)]\underline{1} & 0 \\ -ge^{-i\phi_+}\hat{m}\cdot\underline{\boldsymbol{\sigma}} & 0 & [i\nu_l - \epsilon_{b+}(\mathbf{k})]\underline{1} \end{pmatrix}, \tag{9}$$

where $\hat{m}$ is the polarization direction of the SDW and $\boldsymbol{\sigma}$ are the Pauli matrices in spin space. The order parameter $g(T)$ is real, and the $ab\pm$ matrix elements are assigned arbitrary phases $\phi_{\pm}$. If the CDW was included, then the $b\pm b\mp$ matrix elements would be proportional to the CDW order parameter.[16]

Inverting the inverse Green's function of Eq. (9) yields

$$\underline{G}(\mathbf{k},i\nu_l)=\frac{1}{D(\mathbf{k},i\nu_l)} \times \begin{pmatrix} \underline{1}[i\nu_l-\epsilon_{b+}(\mathbf{k})] \times[i\nu_l-\epsilon_{b-}(\mathbf{k})] & \hat{m}\cdot\boldsymbol{\sigma} g\epsilon^{-i\phi_-}[i\nu_l-\epsilon_{b+}(\mathbf{k})] & \hat{m}\cdot\boldsymbol{\sigma} g e^{-i\phi_+}[i\nu_l-\epsilon_{b-}(\mathbf{k})] \\ \hat{m}\cdot\boldsymbol{\sigma} g e^{-i\phi_-}[i\nu_l-\epsilon_{b+}(\mathbf{k})] & \underline{1}\{[i\nu_l-\epsilon_a(\mathbf{k})] \times[i\nu_l-\epsilon_{b+}(\mathbf{k})]-g^2\} & \underline{1}g^2 e^{i(\phi_+-\phi_-)} \\ \hat{m}\cdot\boldsymbol{\sigma} g e^{-i\phi_+}[i\nu_l-\epsilon_{b-}(\mathbf{k})] & \underline{1}g^2 e^{-i(\phi_+-\phi_-)} & \underline{1}\{[i\nu_l-\epsilon_a(\mathbf{k})] \times[i\nu_l-\epsilon_{b-}(\mathbf{k})]-g^2\} \end{pmatrix}, \tag{10}$$

where the determinant of the inverse Green's function is

$$D(\mathbf{k},i\nu_l)=[i\nu_l-\epsilon_a(\mathbf{k})][i\nu_l-\epsilon_{b+}(\mathbf{k})][i\nu_l-\epsilon_{b-}(\mathbf{k})] -g^2[2i\nu_l-\epsilon_{b+}(\mathbf{k})-\epsilon_{b-}(\mathbf{k})]. \tag{11}$$

Although the $b\pm b\mp$ matrix elements were missing from the inverse Green's function, they now appear in the Green's function of Eq. (10). Each band matrix element of $\underline{G}(\mathbf{k},i\nu_l)$ is proportional to a unit matrix in spin space except $\underline{G}_{ab\pm}$ and $\underline{G}_{b\pm a}$, which are proportional to $\hat{m}\cdot\boldsymbol{\sigma}$. While $\underline{G}_{aa}$ and $\underline{G}_{b\pm b\pm}$ are the diagonal or ''normal'' Green's functions in band space, $G_{ab\pm}\propto g$ and $G_{b\pm b\mp}\propto g^2$ correspond to the ''anomalous'' Green's functions in a superconductor, and vanish above T_N.

The hybridized energies $\epsilon(\mathbf{k})$ are given by the zeros of $D(\mathbf{k},\epsilon)$. These energies are plotted in the solid lines of Figs. 2(a) and 2(b) for the C and I phases, respectively. As expected, energy gaps appear wherever the paramagnetic energies cross. When $g\to 0$, the gaps close and the paramagnetic energies are recovered.

In the C regime, $\epsilon-\epsilon_b(\mathbf{k})$ can be factored from the denominator $D(\mathbf{k},\epsilon)$. When $\partial>0$, the hole Fermi surface is larger than the electron Fermi surface, so there are more holes than electrons. Holes which are not paired to electrons in the CSDW have the unperturbed energies $\epsilon_b(\mathbf{k})$. Since the factor $\epsilon-\epsilon_b(\mathbf{k})$ cancels an identical term in the numerators of the dynamic susceptibilities, these unpaired holes are decoupled from the SDW and do not affect the C spin dynamics. As shall be reported elsewhere,[20] the Coulomb interaction[16] between the paired and unpaired holes may generate a first-order PC transition.

An energy gap of $2\Delta\equiv 2\sqrt{2}g$ centered $z_0/4$ above the chemical potential separates the upper and lower C bands in Fig. 2(b). At $T=0$, $\Delta(0)>z_0/4$, so that the lower band lies completely below the chemical potential. As in a conventional superconductor, the minimum energy 2Δ is needed to break apart an electron-hole pair.

Because the I paramagnetic energies cross at two points, two identical energy gaps appear above and below the central band in Fig. 2(c). The transition across each energy gap is not quite vertical, with the value for z in the middle band slightly smaller in magnitude than on the upper and lower bands. In agreement with infrared data,[21] the I energy gaps are roughly 40% smaller than the C gap, which may make some experiments easier to perform in the I phase. Infrared measurements[21] have also reported indirect transition between the bottom and top bands. At $T=0$, the bottom band again lies completely below the chemical potential. But the middle band intersects the chemical potential at any temperature. So in contrast to the pair-breaking threshold of the C regime, I electron-hole pairs can be broken with zero energy cost. The quasiparticle branches in Fig. 2(c) are numbered so that $\epsilon_1\to\epsilon_a$, $\epsilon_2\to\epsilon_{b+}$, and $\epsilon_3\to\epsilon_{b-}$, as $g\to 0$. Notice that $d\epsilon_1/dz\geq 0$ while $d\epsilon_{2,3}/dz\leq 0$. The CDW in the I phase[16,20] is produced by the Coulomb attraction between electrons and holes on bands 2 and 3.

The Matsubara spin susceptibility $\chi_{\alpha\beta}(\mathbf{q},i\omega_n)$ is defined by

$$\chi_{\alpha\beta}(\mathbf{q},i\omega_n) =\frac{1}{4V}\sum_{\mathbf{k},\mathbf{k}'}\int_0^\beta d\tau\, e^{i\omega_n\tau}\langle T_\tau \underline{\Psi}^\dagger(\mathbf{k}+\mathbf{q},\tau)\cdot\underline{\Lambda}_\beta\cdot\underline{\Psi}(\mathbf{k},\tau) \times\underline{\Psi}^\dagger(\mathbf{k}',0)\cdot\underline{\Lambda}_\alpha\cdot\underline{\Psi}(\mathbf{k}'+\mathbf{q},0)\rangle, \tag{12}$$

where

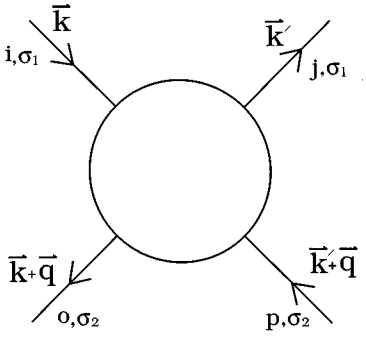

FIG. 3. A graphical representation of the spin-spin correlation function $\chi_{ijop}^{(\sigma_1\sigma_2)}(\mathbf{q},i\omega_n)$.

$$\underline{\Lambda}_\beta = \begin{pmatrix} \underline{\sigma}_\beta & \underline{\sigma}_\beta & \underline{\sigma}_\beta \\ \underline{\sigma}_\beta & \underline{\sigma}_\beta & \underline{\sigma}_\beta \\ \underline{\sigma}_\beta & \underline{\sigma}_\beta & \underline{\sigma}_\beta \end{pmatrix}, \tag{13}$$

$\omega_n = 2n\pi T$ are the boson Matsubara frequencies and V is the volume. The magnetic properties of Cr depend on the transverse and longitudinal spin susceptibilities $\chi_t(\mathbf{q},\omega)$ and $\chi_l(\mathbf{q},\omega)$, defined with respect to the spin-polarization direction $\hat{m}$. No assumptions are made about the angle between $\hat{m}$ and the SDW wave-vector direction $\hat{z}$. As usual, the real-frequency susceptibilities are obtained from the Matsubara susceptibilities with the substitution $\omega_n \rightarrow -i\omega + \epsilon$.

The band- and spin-dependent matrix elements $\chi^{(\sigma_1\sigma_2)}_{ijop}(\mathbf{q},i\omega_n)$ are defined by

$$\chi^{(\sigma_1\sigma_2)}_{ijop}(\mathbf{q},i\omega_n) = \frac{1}{V}\sum_{\mathbf{k},\mathbf{k}'} \int_0^\beta d\tau\, e^{i\omega_n\tau} \langle T_\tau \Psi^\dagger_{o\sigma_2}(\mathbf{k}+\mathbf{q},\tau) \times \Psi_{i\sigma_1}(\mathbf{k},\tau)\Psi^\dagger_{j\sigma_1}(\mathbf{k}',0)\Psi_{p\sigma_2}(\mathbf{k}'+\mathbf{q},0)\rangle. \tag{14}$$

These band matrix elements are represented graphically in Fig. 3, where band indices i, j, o, and p can equal a, $b+$, or $b-$. To simplify our notation, we also define the specific matrix elements

$$\chi_1(\mathbf{q},i\omega_n) = \chi^{\uparrow\uparrow}_{aab+b+}(\mathbf{q},i\omega_n), \tag{15a}$$

$$\chi_2(\mathbf{q},i\omega_n) = \chi^{\uparrow\uparrow}_{b+b+aa}(\mathbf{q},i\omega_n), \tag{15b}$$

$$\chi_3(\mathbf{q},i\omega_n) = \chi^{\uparrow\uparrow}_{b+b-aa}(\mathbf{q},i\omega_n), \tag{15c}$$

$$\chi_4(\mathbf{q},i\omega_n) = \chi^{\uparrow\uparrow}_{aab-b+}(\mathbf{q},i\omega_n), \tag{15d}$$

$$\chi_5(\mathbf{q},i\omega_n) = \chi^{\uparrow\uparrow}_{ab+b+a}(\mathbf{q},i\omega_n), \tag{15e}$$

$$\chi_6(\mathbf{q},i\omega_n) = \chi^{\uparrow\uparrow}_{ab+b-a}(\mathbf{q},i\omega_n), \tag{15f}$$

$$\chi_7(\mathbf{q},i\omega_n) = \chi^{\uparrow\uparrow}_{b+aab+}(\mathbf{q},i\omega_n), \tag{15g}$$

$$\chi_8(\mathbf{q},i\omega_n) = \chi^{\uparrow\uparrow}_{b+aab-}(\mathbf{q},i\omega_n). \tag{15h}$$

Correlation functions with $b\pm \rightarrow b\mp$ are defined by $\overline{\chi_i}(\mathbf{q},i\omega_n)$. For example, $\overline{\chi_1}(\mathbf{q},i\omega_n) = \chi^{\uparrow\uparrow}_{aab-b-}(\mathbf{q},i\omega_n)$.

Within the RPA, each susceptibility is approximated by a series of ladder diagrams with continuous strings of Green's functions forming the two sides of the ladder, and the Coulomb interaction U forming the rungs. Since the Coulomb interaction does not flip the quasiparticle spin, the spin remains unchanged along each side of the ladder. Using the spin symmetries of the Green's functions, any susceptibility with spin variables σ_1 and σ_2 can be related to one of the numerated susceptibilities $\chi_i(\mathbf{q},i\omega_n)$ or $\overline{\chi_i}(\mathbf{q},i\omega_n)$ with both spins up. For example, the ladders for $\chi^{(\sigma_1\sigma_2)}_{aab+b+}(\mathbf{q},i\omega_n)$ must contain an even number of matrix elements like $\underline{G}_{ab\pm}$ and $\underline{G}_{b\pm a}$ on each side. So $\chi^{(\sigma_1\sigma_2)}_{aab+b+}(\mathbf{q},i\omega_n)$ is spin independent, and equals $\chi_1(\mathbf{q},i\omega_n)$. On the other hand, the ladders for $\chi^{(\sigma_1\sigma_2)}_{ab+b+a}(\mathbf{q},i\omega_n)$ must have an odd number of matrix elements $\underline{G}_{ab\pm}$ and $\underline{G}_{b\pm a}$ on each side. Then flipping either σ_1 or σ_2 changes the sign of the susceptibility:

$$\chi^{(\sigma_1,\sigma_2)}_{ab+b+a}(\mathbf{q},i\omega_n) = -\chi^{(-\sigma_1,\sigma_2)}_{ab+b+a}(\mathbf{q},i\omega_n) = -\chi^{(\sigma_1,-\sigma_2)}_{ab+b+a}(\mathbf{q},i\omega_n) = \chi^{(-\sigma_1,-\sigma_2)}_{ab+b+a}(\mathbf{q},i\omega_n),$$

where $\chi^{\uparrow\uparrow}_{ab+b+a}(\mathbf{q},i\omega_n) = \chi_5(\mathbf{q},i\omega_n)$. Thus, every possible correlation function can be related to $\chi_i(\mathbf{q},i\omega_n)$ or $\overline{\chi_i}(\mathbf{q},i\omega_n)$.

It is also straightforward to show that the phases $\phi_\pm$ of the SDW cancel from the ladder diagrams for the susceptibilities. So the arbitrary equilibrium phases do not affect the spin dynamics and can be taken to be zero. However, these phases will be reinstated in Sec. IV in order to interpret the collective modes.

Evaluated to zeroth order in the Coulomb interaction U, the Hartree-Fock (HF) correlation functions are

$$\chi^{(0)}_1(\mathbf{q},i\omega_n) = -\frac{T}{V}\sum_{l,\mathbf{k}} G^{\uparrow\uparrow}_{aa}(\mathbf{k},i\nu_l) G^{\uparrow\uparrow}_{b+b+}(\mathbf{k}+\mathbf{q},i\nu_l - i\omega_n), \tag{16a}$$

$$\chi^{(0)}_2(\mathbf{q},i\omega_n) = -\frac{T}{V}\sum_{l,\mathbf{k}} G^{\uparrow\uparrow}_{b+b+}(\mathbf{k},i\nu_l) G^{\uparrow\uparrow}_{aa}(\mathbf{k}+\mathbf{q},i\nu_l - i\omega_n), \tag{16b}$$

$$\chi^{(0)}_3(\mathbf{q},i\omega_n) = -\frac{T}{V}\sum_{l,\mathbf{k}} G^{\uparrow\uparrow}_{b+b-}(\mathbf{k},i\nu_l) G^{\uparrow\uparrow}_{aa}(\mathbf{k}+\mathbf{q},i\nu_l - i\omega_n), \tag{16c}$$

$$\chi^{(0)}_4(\mathbf{q},i\omega_n) = -\frac{T}{V}\sum_{l,\mathbf{k}} G^{\uparrow\uparrow}_{aa}(\mathbf{k},i\nu_l) G^{\uparrow\uparrow}_{b+b-}(\mathbf{k}+\mathbf{q},i\nu_l - i\omega_n), \tag{16d}$$

$$\chi^{(0)}_5(\mathbf{q},i\omega_n) = -\frac{T}{V}\sum_{l,\mathbf{k}} G^{\uparrow\uparrow}_{ab+}(\mathbf{k},i\nu_l) G^{\uparrow\uparrow}_{ab+}(\mathbf{k}+\mathbf{q},i\nu_l - i\omega_n), \tag{16e}$$

$$\chi^{(0)}_6(\mathbf{q},i\omega_n) = -\frac{T}{V}\sum_{l,\mathbf{k}} G^{\uparrow\uparrow}_{ab+}(\mathbf{k},i\nu_l) G^{\uparrow\uparrow}_{ab-}(\mathbf{k}+\mathbf{q},i\nu_l - i\omega_n). \tag{16f}$$

Since the Green's functions $G^{\uparrow\uparrow}_{ab\pm} = G^{\uparrow\uparrow}_{b\pm a}$ are symmetric, $\chi^{(0)}_7(\mathbf{q},i\omega_n) = \chi^{(0)}_5(\mathbf{q},i\omega_n)$ and $\chi^{(0)}_8(\mathbf{q},i\omega_n) = \chi^{(0)}_6(\mathbf{q},i\omega_n)$. Using the symmetry between the $b\pm$ energies in Eqs. (3), it is easy to show that

$$\overline{\chi^{(0)}_i}(\mathbf{q},i\omega_n) = \chi^{(0)}_i(-\mathbf{q},i\omega_n). \tag{17}$$

Only $\chi^{(0)}_1(\mathbf{q},i\omega_n)$ and $\chi^{(0)}_2(\mathbf{q},i\omega_n)$ are nonzero above T_N.

After performing the analytic continuation $i\omega_n \rightarrow \omega + i\varepsilon$, each HF susceptibility can be expressed in real and imaginary parts as

$$\chi^{(0)}_i(\mathbf{q},\omega+i\varepsilon) = \phi^{(i)}_1(\mathbf{q},\omega) + i\phi^{(i)}_2(\mathbf{q},\omega). \tag{18}$$

Since the imaginary susceptibilities vanish when $\omega = 0$, the real part $\phi^i_1(\mathbf{q},0)$ is obtained by setting $\omega_n = 0$ in Eqs. (16a)–(16f). The imaginary part $\phi^{(i)}_2(\mathbf{q},\omega)$ can be evaluated by integrating over a spectral density[12,22] that involves all possible quasiparticle transitions between branches 1, 2, and 3 with momentum difference $\xi \equiv cq$ and energy difference ω. If a quasiparticle transition is allowed between branches i and j, then the imaginary susceptibility will contain an integral of the form

$$I(q,\omega)=\int dv\ F(v)\delta[z_i(v)-z_j(v-\omega)-cq]$$
$$=\frac{F(v)}{|dg_{ij}/dv|}\bigg|_{v*}, \tag{19}$$

where $g_{ij}(v)\equiv z_i(v)-z_j(v-\omega)$, and v^* satisfies the momentum conservation condition

$$z_i(v^*)-z_j(v^*-\omega)=cq. \tag{20}$$

In Appendix A, the frequencies v^* and energies z_i satisfying Eq. (20) are solved analytically for both the C and I regimes. Finally, the frequency dependence of each real susceptibility is obtained from the Kramers-Kronig relation

$$\phi_1^{(i)}(\mathbf{q},\omega)-\phi_1^{(i)}(\mathbf{q},0)=\frac{\omega}{\pi}\int_{-\infty}^{\infty}\frac{d\omega'}{\omega'}\frac{\phi_2^{(i)}(\mathbf{q},\omega')}{\omega'-\omega}. \tag{21}$$

The zero-frequency real HF susceptibilities are derived in Appendix B; the imaginary HF susceptibilities are derived in Appendix C. Symmetry relations between the HF susceptibilities are provided in Appendix D.

In this and the following papers, we evaluate the transverse and longitudinal susceptibilities $\chi_t(\mathbf{q},\omega)$ and $\chi_l(\mathbf{q},\omega)$ in terms of the six HF susceptibilities. The neutron-scattering cross sections are then given by

$$\sigma_t=U^2N(0)(n+1)\mathrm{Im}\chi_t(\mathbf{q},\omega), \tag{22a}$$

$$\sigma_l=U^2N(0)(n+1)\mathrm{Im}\chi_l(\mathbf{q},\omega), \tag{22b}$$

where $n=1/[\exp(\beta\omega)-1]$ is the Boltzmann function. Because χ_t and χ_l are each proportional to $1/U^2N(0)$, the cross sections defined above are independent of both the Coulomb interaction U and the single-spin density of states $N(0)$. Above T_N, $\chi_t(\mathbf{q},\omega)=2\chi_l(\mathbf{q},\omega)$ and $\sigma_t=2\sigma_l$, so that spin fluctuations are isotropic.

When (q,ω) joins quasiparticle energies with the same slope, such as the filled circles in Fig. 2(b), the denominator dg_{ij}/dv of $I(q,\omega)$ vanishes, and the imaginary HF susceptibilities diverge. This produces either a divergence or a zero in the transverse and longitudinal susceptibilities. Often a cusp or divergence in one susceptibility coincides with a zero in the other. Such quasiparticle transitions are said to be *enhanced*. Because nearby transitions have very small derivatives dg_{ij}/dv, the most important enhanced transitions join points with zero slope, such as the vertical transition between the empty circles in Fig. 2(b).

If q is measured from a SDW wave vector, then a transverse or longitudinal collective mode with frequency ω' and wave vector $\xi'=cq'$ corresponds to a pole of the cross section

$$\sigma(\xi,\omega)=\frac{1}{1-e^{-\beta\omega}}\ \mathrm{Im}\ \frac{1}{t_1+it_2}=\frac{-1}{1-e^{-\beta\omega}}\frac{t_2}{t_1^2+t_2^2}, \tag{23}$$

with $t_1(\xi',\omega')=t_2(\xi',\omega')=0$. Should $t_2\leqslant 0$ vanish faster than t_1, the cross section will contain a δ function,

$$\sigma=\pi\frac{1}{1-e^{-\beta\omega'}}\ \delta(t_1)+\cdots. \tag{24}$$

For most collective modes, the real denominator t_1 can be linearized about the wave vector ξ' at a fixed frequency ω'. So if $t_1=\alpha(\xi-\xi')$, the strength of the mode integrated over ξ is given by

$$s=\frac{\pi}{|\alpha|}\frac{1}{1-e^{-\beta\omega'}}. \tag{25}$$

The dispersion of a damped excitation with $t_2<0$ is fixed by the condition $t_1(\xi',\omega')=0$ and its half-width is given by $\Delta\xi=|t_2/\alpha|$, which vanishes as $t_2\to 0$. Although the excitation is broadened by the damping energy $t_2<0$, its integrated weight is still given by Eq. (25) and is independent of t_2. Because $\alpha\propto d\omega/d\xi$, the weight of any damped excitation or collective mode diverges when $d\omega/d\xi=0$.

III. COMMENSURATE FORMALISM

Since the C hole energies $\epsilon_{b\pm}(\mathbf{k})$ are identical, the two- and three-band models for the dynamics of C Cr alloys are equivalent. In order to employ the same notation for the C and I phases, however, we shall use the three-band model for the C dynamics. As discussed in Sec. I, the spin dynamics of γ-Mn alloys also builds on the basic formalism developed in this section.

Using the relations between the $ab\pm$ and $b\pm b\mp$ matrix elements of the Green's function, we find that the transverse and longitudinal spin susceptibilities of Eq. (12) each contain six terms:

$$\chi_t(\mathbf{q},\omega)=4[\chi_1(\mathbf{q},\omega)+\chi_2(\mathbf{q},\omega)+\chi_3(\mathbf{q},\omega)+\chi_4(\mathbf{q},\omega)]$$
$$-8[\chi_5(\mathbf{q},\omega)+\chi_6(\mathbf{q},\omega)], \tag{26}$$

$$\chi_l(\mathbf{q},\omega)=2[\chi_1(\mathbf{q},\omega)+\chi_2(\mathbf{q},\omega)+\chi_3(\mathbf{q},\omega)+\chi_4(\mathbf{q},\omega)]$$
$$+4[\chi_5(\mathbf{q},\omega)+\chi_6(\mathbf{q},\omega)]. \tag{27}$$

The relative sign difference between the transverse and longitudinal susceptibilities arises from the symmetry relation $G^{\uparrow\uparrow}_{ab\pm}(\mathbf{q},\omega)=-G^{\downarrow\downarrow}_{ab\pm}(\mathbf{q},\omega)$.

After every susceptibility is expanded in a series of ladder diagrams, each subset $\{\chi_1,\chi_4,\chi_6\}$ and $\{\chi_2,\chi_3,\chi_5\}$ only couples to terms within itself:

$$\chi_1=\chi_1^{(0)}+\chi_1^{(0)}U\chi_1+\chi_4^{(0)}U\chi_4+2\chi_5^{(0)}U\chi_6, \tag{28a}$$

$$\chi_4=\chi_4^{(0)}+\chi_1^{(0)}U\chi_4+\chi_4^{(0)}U\chi_1+2\chi_5^{(0)}U\chi_6, \tag{28b}$$

$$\chi_6=\chi_6^{(0)}+\chi_6^{(0)}U(\chi_1+\chi_4)+(\chi_2^{(0)}+\chi_3^{(0)})U\chi_6, \tag{28c}$$

and

$$\chi_2=\chi_2^{(0)}+\chi_2^{(0)}U\chi_2+\chi_3^{(0)}U\chi_3+2\chi_6^{(0)}U\chi_5, \tag{29a}$$

$$\chi_3=\chi_3^{(0)}+\chi_2^{(0)}U\chi_3+\chi_3^{(0)}U\chi_2+2\chi_6^{(0)}U\chi_5, \tag{29b}$$

$$\chi_5=\chi_5^{(0)}+\chi_5^{(0)}U(\chi_2+\chi_3)+(\chi_1^{(0)}+\chi_4^{(0)})U\chi_5. \tag{29c}$$

The first set of three equations is sketched graphically in Fig. 4, where the boxes represent the HF susceptibilities and the circles represent the full susceptibilities. Adding Eq. (28a) with (28b) and Eq. (29a) with (29b) gives the same set of four equations that would arise from a two-band model.[17]

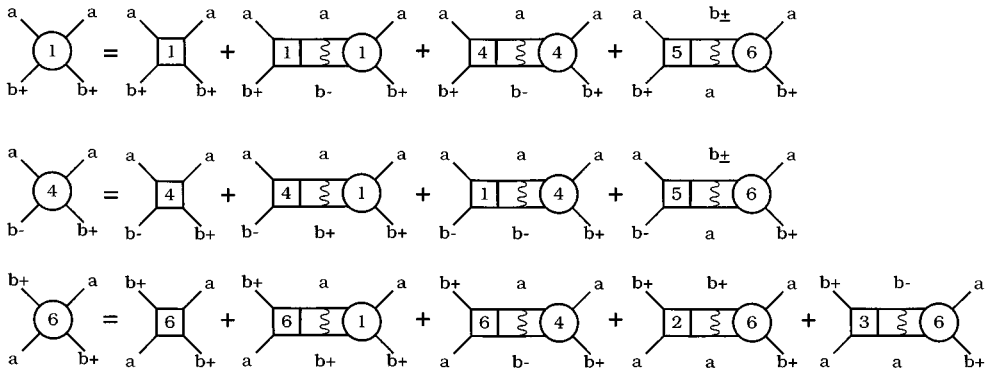

FIG. 4. Graphical representation of the coupled equations for $\chi_1(\mathbf{q},\omega)$, $\chi_4(\mathbf{q},\omega)$, and $\chi_6(\mathbf{q},\omega)$ in C alloys.

Using the relations between the HF susceptibilities in Appendixes B and C, we find that $\chi_5(\mathbf{q},\omega)=\chi_6(\mathbf{q},\omega)$ and $\chi_1(\mathbf{q},\omega)+\chi_4(\mathbf{q},\omega)=\chi_2(\mathbf{q},\omega)+\chi_3(\mathbf{q},\omega)$.

In terms of the variables

$$\Psi_{\pm}(\mathbf{q},\omega)=\chi_1(\mathbf{q},\omega)+\chi_4(\mathbf{q},\omega)\pm 2\chi_5(\mathbf{q},\omega), \tag{30}$$

the transverse and longitudinal susceptibilities are

$$\chi_t(\mathbf{q},\omega)=8\frac{\Psi_-(\mathbf{q},\omega)}{1-U\Psi_-(\mathbf{q},\omega)}=-\frac{8}{U}+\frac{8}{U}\frac{1}{1-U\Psi_-(\mathbf{q},\omega)}, \tag{31a}$$

$$\chi_l(\mathbf{q},\omega)=4\frac{\Psi_+(\mathbf{q},\omega)}{1-U\Psi_+(\mathbf{q},\omega)}=-\frac{4}{U}+\frac{4}{U}\frac{1}{1-U\Psi_+(\mathbf{q},\omega)}. \tag{31b}$$

If the real and imaginary parts of $\Psi_{\pm}(\mathbf{q},\omega)$ are defined by $\Psi_{\pm}=\Psi_{\pm 1}+i\Psi_{\pm 2}$, then the results in Appendixes B and C can be summarized as

$$\Psi_{\pm 1}(\mathbf{q},0)=\frac{1}{U}-2\pi iTN(0)[(cq)^2+2\Delta^2\pm 2\Delta^2]\times\sum_l\frac{\mathrm{sgn}(\nu_l)}{x_l[x_l^2-(cq)^2]},\quad T<T_N. \tag{32}$$

$$x_l=\left[\left(\frac{z_0}{2}-2i\nu_l\right)^2-4\Delta^2\right]^{1/2}, \tag{33}$$

$$\Psi_{\pm 2}(\mathbf{q},\omega)=-\frac{\pi}{4}N(0)\{\theta[(cq)^2-\omega^2]+\theta[\omega^2-(cq)^2-4\Delta^2]\}\left(\frac{(cq)^2+4\Delta^2-\omega^2}{(cq)^2-\omega^2}\right)^{\pm 1/2}\times\left\{f\left(v+\frac{z_0}{4}\right)-f\left(v+\frac{z_0}{4}-\omega\right)-f\left(-v+\frac{z_0}{4}\right)+f\left(-v+\frac{z_0}{4}+\omega\right)\right\}, \tag{34}$$

where $\mathrm{sgn}\,\mathrm{Im}(x_l)=-\mathrm{sgn}(\nu_l)$, $f(z)=1/[\exp(\beta z)+1]$ is the Fermi function, $\theta(x)$ is the step function, and

$$v=\frac{\omega}{2}+\frac{cq}{2}\left(\frac{(cq)^2+4\Delta^2-\omega^2}{(cq)^2-\omega^2}\right)^{1/2}. \tag{35}$$

The frequency dependences of the real parts $\Psi_{\pm 1}(\mathbf{q},\omega)$ are evaluated using the Kramers-Kronig relation of Eq. (21). Above T_N, the additional term $-N(0)\ln(T/T_N)$ must be added to Eq. (32).

IV. COMMENSURATE DYNAMICS

The imaginary susceptibilities $\Psi_{\pm 2}(\mathbf{q},\omega)$ are generated by quasiparticle transitions with frequency ω and wave vector $\mathbf{q}$. For any nonzero wave vector, quasiparticle transitions within the lower or upper band are allowed when $\omega<cq$. When $q=0$, transitions between the lower and upper bands are only possible above a pair-breaking energy of 2Δ. When $q>0$ is fixed, the interband transition with the smallest frequency connects the filled circles of Fig. 2(b) with $\omega=2\sqrt{\Delta^2+(cq)^2/4}$. These restrictions are enforced by the θ functions in Eq. (34).

Regions with allowed quasiparticle transitions lie outside the shaded borders of Fig. 5. Above the top border and below the bottom border, transverse and longitudinal spin fluctuations are intrinsically damped even in the absence of impurity or electron-phonon scattering. Inside the shaded borders, however, quasiparticle transitions are disallowed, the imaginary HF susceptibilities are zero, and the neutron-scattering cross sections must vanish.

From Eqs. (31a) and (31b), the transverse and longitudinal mode frequencies are zeros of the functions

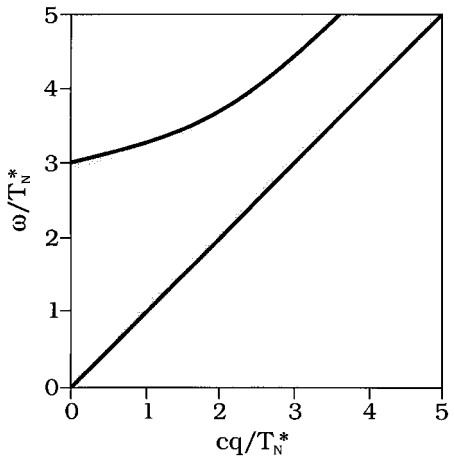

FIG. 5. Transverse and longitudinal C mode frequencies bordering regions of incoherent excitations outside the hashed region for $T=0.5T_N$ and $z_0/T_N^*=4$.

$$1-U\Psi_{\mp}(\mathbf{q},\omega)=(1-U\Psi_{\mp 1}(\mathbf{q},\omega))-iU\Psi_{\mp 2}(\mathbf{q},\omega)=0. \tag{36}$$

As proven in Appendix E, these conditions have the very simple solutions

$$\omega_t=cq, \tag{37}$$

$$\omega_l=2\sqrt{\Delta^2+(cq)^2/4}, \tag{38}$$

which coincide with the borders of the quasiparticle continuum in Fig. 5. Because the $b\pm$ hole energies have been translated by momentum $\mathbf{Q}'=(G/2)\hat{z}$, q is measured from the CSDW wave vector $(G/2)\hat{z}$. Hence the crystal momentum corresponding to $\mathbf{q}$ is $\mathbf{p}=\mathbf{q}+(G/2)\hat{z}$. Whereas the transverse mode frequency is independent of the temperature and energy mismatch, the longitudinal mode frequency depends on both T and z_0 through the energy gap $\Delta=\sqrt{2}g$. As $T\rightarrow T_N$, $\Delta\rightarrow 0$ and $\omega_l\rightarrow\omega_t$. So above T_N, incoherent quasiparticle transitions are allowed at all frequencies and wave vectors.

The collective modes in the C phase can be associated with fluctuations of the CSDW. Starting with the inverse Green's function of Eq. (9) with arbitrary phases $\phi_{\pm}$, the equilibrium spin at lattice site $\mathbf{R}$ can be written

$$\begin{aligned}\mathbf{S}_0(\mathbf{R})&=\alpha_s g\hat{m}\{\cos(\mathbf{Q}'\cdot\mathbf{R}+\phi_+)+\cos(\mathbf{Q}'\cdot\mathbf{R}+\phi_-)\}\\&=2\alpha_s g\hat{m}(-1)^{2R_z/a}\cos\phi_{\rm av}\cos\theta/2,\end{aligned} \tag{39}$$

where $\phi_{\rm av}=(\phi_++\phi_-)/2$ is the average phase and $\theta=\phi_+-\phi_-$ is the phase difference. The constant of proportionality is $\alpha_s=-2\hbar V/UN$, where $U>0$ is the Coulomb interaction and N is the number of atoms. Of course, the actual spin density has the same spatial distribution as the d-band electrons. But due to the rather localized orbitals of those electrons, Eq. (39) is a good approximation.

Although the amplitude $\alpha_s g$ of each SDW is fixed by the thermodynamic free energy, the phases $\phi_{\pm}$ are not. Whereas the average phase $\phi_{\rm av}$ remains undetermined in either the C or I phases, the phase difference θ in the C phase is fixed at $\pi/2+n\pi$ (n any integer) by charge conservation.[20] It seems likely that spin-orbit coupling will further act to maximize the spin on every lattice site, thereby fixing $|\cos\phi_{\rm av}|=1$. Then the magnitude of the spin would be given by $\sqrt{2}\alpha_s g$.

While the transverse modes of Eq. (37) correspond to fluctuations in the polarization direction $\hat{m}$, the longitudinal excitations of Eq. (38) correspond to fluctuations in the SDW amplitude $g|\cos\phi_{\rm av}\cos\theta/2|$. For the I phase discussed in paper II, the phase difference θ remains arbitrary and fluctuations in θ are responsible for a class of Goldstone modes called phasons. But for the C phase, fluctuations in θ are equivalent to fluctuations in the SDW amplitude so phason modes are absent.

A. Spin-wave modes

Associated with the rotational symmetry of the SDW about the $\hat{m}$ direction, transverse SW's are Goldstone modes which evolve from the SDW ordering wave vector. As first predicted by Fedders and Martin[11] for $T=0$ and $z_0=0$, the SW mode velocity is $q=v_F/\sqrt{3}$. Liu[12] later extended this result to perfectly nested Cr with $z_0=0$ at any temperature. Walker[13] obtained the same SW velocity for all values of z_0 at $T=0$. Finally, we have shown that the SW mode velocity is independent of both temperature and mismatch energy. Whereas SW's in a transition-metal ferromagnet[23] like Ni are damped at very low frequencies by the excitation of electron-hole pairs, SW's in a transition-metal antiferromagnet are undamped at any frequency within the RPA.

However, our results disagree with Sato and Maki,[24] who included explicit damping terms in a two-band model near the Néel temperature. Although their expressions for the Matsubara susceptibilities $\Psi_{\pm}(\mathbf{q},i\omega_n)$ are identical to ours, their solutions for the CSW modes are quite different. Sato and Maki find that the SW velocity vanishes as $T\rightarrow T_N$ or as z_0 approaches the triple point.

Several workers[25–27] have studied the spin dynamics of both CSDW and ISDW states using phenomenological expansions of the free energy in powers of the magnetization near T_N. The local-spin operator $\mathbf{S}(\mathbf{R})$ then obeys the canonical spin commutation rules. All such phenomenological models predict that the SW velocity is proportional to the SDW order parameter g and vanishes as $T\rightarrow T_N$. However, such phenomenological expansions have no justification for itinerant antiferromagnets. In particular, there is no reason to expect that the spin $\mathbf{S}(\mathbf{R})$ obeys the commutation rules for Heisenberg spins.

Because the magnetic moments of an itinerant antiferromagnet are not fixed in magnitude, there has been some question[28] whether the SW modes in Cr are similar to the SW modes in a local-moment antiferromagnet. However, the fluctuation of the magnetic moment at any lattice site costs an energy of at least 2Δ. So low-frequency SW's can exist only if each spin $\mathbf{S}(\mathbf{R})$ rotates rigidly about its equilibrium position $\mathbf{S}_0(\mathbf{R})$. Form-factor measurements by Sinha *et al.*[4] confirm that the magnetic moments of Cr do not fluctuate in magnitude at frequencies below about 17 meV.

The cross section of the SW modes about a CSDW state is given analytically by the remarkably simple result

$$\sigma_{\rm sw}(\mathbf{q},\omega)=(n+1)\,\frac{16\pi\Delta^2}{\omega}\,\delta(\omega-cq), \tag{40}$$

which has precisely the same form[29] as for a local-moment antiferromagnet. So the dynamical susceptibilities of the SW modes in itinerant and local-moment antiferromagnets are virtually identical. Integrating this cross section over $\xi=cq$, we find that the SW strength defined by Eq. (25) is

$$s_t=(n+1)\,\frac{16\pi\Delta^2}{\omega}. \tag{41}$$

As expected, s_t vanishes at the Néel temperature. More unexpectedly, s_t depends on the mismatch energy z_0 only through the energy gap Δ. Notice that the normalized strength $s_t/(n+1)$ falls off inversely with frequency. The decrease in the SW strength $s_t\sim\Delta^2$ with temperature was observed by Sinha *et al.*[4]

Since $c\propto v_F$, the SW velocity in Cr is about 50 times larger than in a rare-earth antiferromagnet. This greatly complicates the measurement of the SW velocity by neutron scattering, which has a resolution[9] in q space larger than the splitting between the SW peaks. While SW modes have been clearly observed in γ-Mn alloys,[19] only one experiment[3] on CrMn alloys has resolved the splitting of the central peak at

27 meV. Instead, most measurements observe the broadening of the central peak with frequency. Fits[2,3] to the width of this ''chimney'' indicate that the SW velocity is roughly 33% smaller than the theoretical SW velocity of $v_F/\sqrt{3}\approx 1500$ meV Å or about 2.3×10^7 cm/s.

To explain this disagreement, Liu[28] proposed a ''frozen magnon'' model which constrains the magnitudes of the local magnetic moments $\mathbf{S}(\mathbf{R})$, and assumes that the spin deviation induced by a single SW is the same as for a conventional antiferromagnet. This approach yields the renormalized SW velocity $\sqrt{2UN(0)}c\approx 0.55c$, in closer agreement with experiments than the RPA result. Since SW's within the RPA also preserve the magnitude of the spin $\mathbf{S}(\mathbf{R})$ on each lattice site, the other assumption of the ''frozen magnon'' model may renormalize the SW mode velocity. As discussed below and in the conclusion to paper II, the discrepancy between the observed and predicted SW velocities can also be explained within the RPA.

B. Amplitude modes

Fluctuations in the SDW amplitude g are caused by the separation and formation of electron-hole pairs. So $q=0$ fluctuations with the same periodicity as the CSDW cost pair-breaking energy 2Δ. Amplitude modes in an itinerant antiferromagnet were first predicted within the Hubbard model by Sokoloff,[30] whose result differs slightly from Eq. (38) but agrees in the $q=0$ limit. To order q^2, our result agrees with Psaltakis,[31] who used a one-band model for perfectly nested Cr at $T=0$. For small q, Eq. (38) also coincides with the amplitude mode frequency of a conventional superconductor.[32]

As shown in Fig. 5, the amplitude and SW modes *never intersect*, and become nearly parallel for large wave vectors. Since the lower boundary of the particle-hole continuum coincides with the mode frequency ω_l, the longitudinal mode is undamped at any wave vector. By contrast, the longitudinal amplitude mode of a superconductor is immediately damped[32] as it enters the quasiparticle continuum above 2Δ for any nonzero wavevector

After expanding the imaginary susceptibility for small q, Psaltakis[31] concluded that the damping energy of the amplitude mode is proportional to $c|q|$. We have reproduced Psaltakis' result by first setting $\mathbf{q}=0$ in the imaginary susceptibility $\Psi_{+2}(\mathbf{q},\omega)$ and only then setting $\omega=\omega_l(q)$. However, this procedure neglects the explicit q dependence of the longitudinal susceptibility.

A zero of the denominator $t_1+it_2\propto 1-U\Psi_{\mp}(\mathbf{q},\omega)$ at wave vector $\xi'=cq'$ and fixed frequency ω is associated with a δ function in the susceptibility, provided that the real part $t_1\propto 1-U\Psi_{\mp 1}(\mathbf{q},\omega)$ vanishes linearly as $U(\xi-\xi')$, and that the imaginary part $t_2\propto -U\Psi_{\mp 2}(\mathbf{q},\omega)$ is much smaller than t_1 near ξ'. Due to the Fermi functions in Eq. (34), $\Psi_{-2}(\mathbf{q},\omega)$ vanishes exponentially fast as $\xi\rightarrow\omega^+$; due to the θ functions, $\Psi_{-2}(\mathbf{q},\omega)$ is infinitesimally small as $\xi\rightarrow\omega^-$. On either side of $\xi=\omega$, $1-U\Psi_{-1}(\mathbf{q},\omega)$ is proportional to $U(\xi-\omega)$. So the zero of the transverse denominator at the SW frequency ω_t is indeed associated with a δ function in the transverse susceptibility.

For the longitudinal amplitude mode at $\omega_l(\mathbf{q})$, this is not the case. When ω is fixed, the longitudinal mode appears at the wave vector $\xi=\zeta(\omega)\equiv\sqrt{\omega^2-4\Delta^2}$. As $\xi\rightarrow\zeta^-$, $\Psi_{+2}(\mathbf{q},\omega)$ vanishes much more slowly than the real part $1-U\Psi_{+1}(\mathbf{q},\omega)\propto U(\xi-\zeta)$. As $\xi\rightarrow\zeta^+$, $1-U\Psi_{+1}(\mathbf{q},\omega)$ is proportional to $U(\xi-\zeta)^\alpha$ with $\alpha<1$. So on either side of $\xi=\zeta(\omega)$, the pole in the longitudinal susceptibility is not associated with a δ function.[23] Unlike the SW δ function, the weight of the amplitude mode is completely contained within the incoherent background. Moreover, the absence of a longitudinal δ function implies that oscillations of the CSDW amplitude decay with time according to a power law, as predicted by Volkov and Kogan[33] for the $\mathbf{q}=0$ amplitude oscillations of a superconductor.

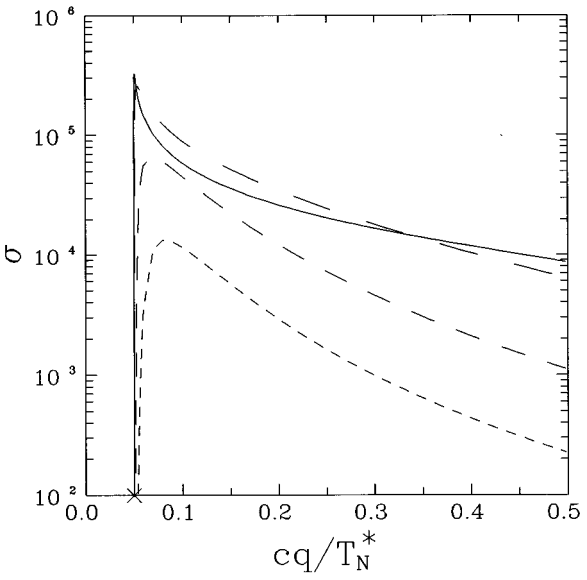

FIG. 6. The total C cross section vs cq/T_N^* for $z_0=4T_N^*$, $\omega=0.05T_N^*$, and $T/T_N=0.974$ (solid), 0.9 (long dash), 0.6 (medium dash), or 0.4 (short dash). The SW δ function is denoted by an X.

C. Cross sections and incoherent background

As defined by Eqs. (22), the transverse and longitudinal cross sections are independent of both the Coulomb interaction U and the density of states $N(0)$. In the C phase, transverse and longitudinal spin fluctuations cannot be distinguished. So in Figs. 6 and 7, we plot the total cross section $\sigma=\sigma_t+\sigma_l$ versus wave vector for $z_0=4T_N^\star$ and $\omega/T_N^\star=0.05$ or 2.0. Here, $T_N^\star\approx 80$ meV is the fictitious Néel temperature[11] of a perfectly nested alloy with $\partial=0$. It is defined by Eq. (B12) in terms of the energy cutoff ϵ_0 and the Coulomb interaction U. The zero-temperature energy gap in the C phase is then given by the BCS result $\Delta(0)=1.764T_N^\star$. The δ-function contribution of each SW at $\xi=\omega$ is denoted by an X in these two figures.

Since ω is smaller than the pair-breaking threshold $2\Delta(T)$ in Fig. 6, no excitations are possible for $\xi<\omega$. Just above $\xi=\omega$, longitudinal fluctuations vanish and transverse fluctuations dominate. When $\omega>2\Delta(T)$, the cross section contains contributions from both $\xi<\zeta(\omega)$ and $\xi>\omega$. The pair-breaking regime below ζ appears in Fig. 7 for $T/T_N=0.9$ or 0.975. Longitudinal fluctuations dominate just below the pair-breaking edge at $\xi=\zeta$. In fact, all the weight of the amplitude mode is contained in the divergence of σ_l below $\zeta(\omega)$.

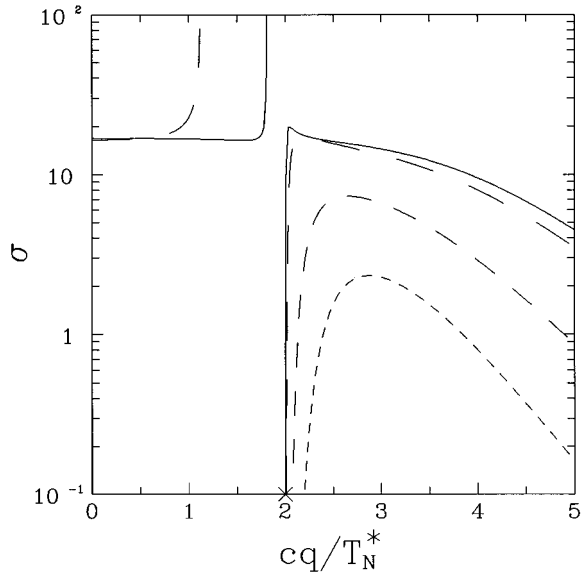

FIG. 7. Same as Fig. 6, but with $\omega=2T_N^*$.

The integrated weight of the incoherent background is defined by

$$I_i(\omega)=\int_{-\infty}^{\infty} d\xi\ \sigma_i(\xi,\omega), \tag{42}$$

where $\sigma_i(\xi,\omega)$ excludes the δ-function contributions of the SW modes. In Fig. 8, we plot the integrated background I_i versus T/T_N for $\omega/T_N^\star=3$. Since it is produced by thermally-excited quasiparticle transitions, the incoherent background vanishes at $T=0$ and grows monotonically with temperature. At sufficiently small temperatures that $2\Delta(T)>\omega$, only intraband transitions contribute to this background. When the temperature is large enough that $2\Delta(T)<\omega$, quasiparticle transitions between the lower and upper bands are allowed.

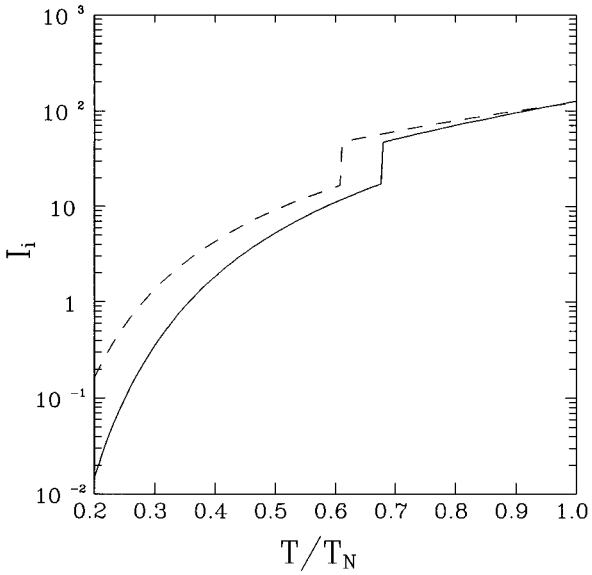

FIG. 8. The incoherent C background I_i vs T/T_N for $\omega=3T_N^*$ and $z_0/T_N^*=0$ (solid) or 4 (dash).

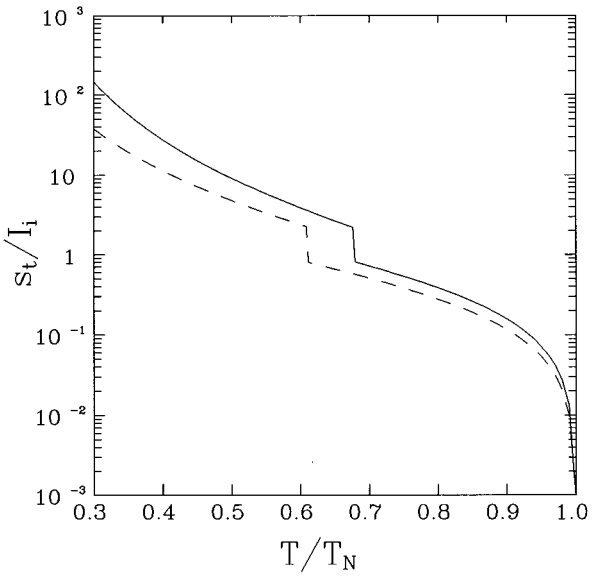

FIG. 9. The relative SW strength s_t/I_i vs T/T_N for the same parameters as Fig. 8.

Due to the divergence of the longitudinal cross section below $\xi=\zeta(\omega)$, the background increases discontinuously at the pair-breaking threshold. As the energy mismatch z_0 decreases, the minimum in the nesting free energy becomes deeper, and incoherent fluctuations are suppressed. Consequently, the integrated background is smaller for $z_0=0$ than for $z_0=4T_N^\star$. But at T_N, the integrated paramagnetic background is relatively independent of z_0.

While the incoherent background increases with temperature, the relative SW strength s_t/I_i plotted in Fig. 9 for $\omega/T_N^*=3$ decreases. At $T=0$, $I_i=0$, so the relative SW strength diverges. At a temperature of $0.5T_N$, the strength of *each* SW is still several times larger than the incoherent background. For both $z_0=0$ and $z_0=4T_N^*$, the relative SW strength s_t/I_i falls below 1 when $2\Delta(T)$ becomes smaller than ω. Only for temperatures above about $0.8T_N$ does the SW strength become negligible compared to the background.

Since the incoherent background peaks at a larger wave vector than the SW δ function, Fig. 9 suggests that the total cross section will peak at a higher wave vector than the SW mode. Because the incoherent background grows with temperature, the observed SW velocity will decrease as the temperature increases. For temperatures above about $0.6T_N$. the observed SW velocity may be substantially smaller than the true mode velocity c. However, systematic measurements of the SW velocity as a function of frequency and temperature are needed to confirm this explanation for the discrepancy between the observed and theoretical mode velocities. Another possible explanation for this discrepancy is proposed in the conclusion to paper II.

Above T_N, the SW δ functions are absent, and incoherent spin fluctuations generate the paramagnetic background[24,34] which was most recently reported by Fawcett *et al.*[35] and Noakes *et al.*[36] The paramagnetic cross section just above T_N is much smaller than the cross section just below T_N due to both the rapid falloff in the SW intensities near T_N and to the extra $\ln(T/T_N)$ term in Eq. (32), which removes the zero-frequency divergence of the susceptibility.

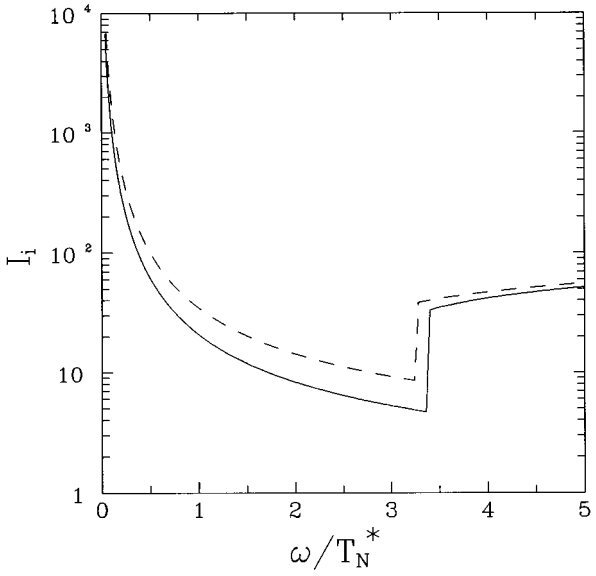

FIG. 10. The incoherent C background I_i vs normalized frequency ω/T_N^* for $T=0.5T_N$ and $z_0/T_N^*=0$ (solid) or 4 (dash).

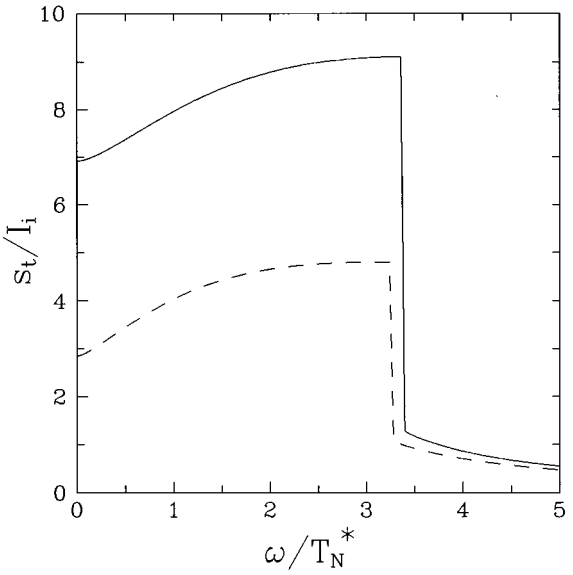

FIG. 11. The relative SW strength s_t/I_i vs ω/T_N^* for the same parameters as in Fig. 10.

Also of experimental interest are results at a fixed temperature as a function of frequency. In Fig. 10, we plot the background cross section versus frequency for $T/T_N=0.5$. Although the imaginary susceptibilities $\Psi_{\pm 2}(\mathbf{q},\omega)$ vanish as $\omega\rightarrow 0$, the cross section remains nonzero due to the Boltzmann factor $n+1=1/[1-\exp(-\beta\omega)]\rightarrow T/\omega$ in Eqs. (22). It is apparent from Fig. 10, however, that the integrated background diverges more strongly than the Boltzmann factor $n+1$. Due to the divergence of the transverse susceptibility at the SDW ordering wave vector, the normalized background $I_i/(n+1)$ diverges like $1/\omega$ below T_N. The incoherent background initially decreases with frequency but then increases discontinuously at $\omega=2\Delta(T)$ due to the onset of amplitude fluctuations. Beyond this point, the background continues to increase with frequency as the amplitude fluctuations grow.

Since both the integrated background I_i and the SW strength s_t diverge at zero frequency like $(n+1)/\omega\propto T/\omega^2$, the ratio s_t/I_i approaches a finite value as $\omega\rightarrow 0$. As shown in Fig. 11, the relative SW strength reaches a maximum just below the pair-breaking threshold $\omega=2\Delta$. Above this threshold, the relative strength of each SW drops dramatically and continues to decrease with increasing frequency. For all frequencies, Figs. 10 and 11 indicate that the incoherent background decreases and the relative SW strength increases as z_0 decreases and the nesting improves.

An examination of Figs. 9 and 11 reveals that the two SW modes dominate the incoherent background at low temperatures and small frequencies. More precisely, $2s_t/I_t\gg 1$ when $\omega<2\Delta(T)$. In practice, this means that virtually all measurements on C alloys can be simply described by Eqs. (39) and (40) for the cross section and strength of the SW modes. Only at very high frequencies or close enough to the Néel temperature that $\omega>2\Delta(T)$ does the incoherent background play a significant role.

Recent low-frequency and low-temperature measurements by Lorenzo *et al.*[9] in the I phase indicate that the peak intensities at the SDW satellites depend on temperature mainly through the Boltzmann factor $n+1$. At fixed values of q and ω, the transverse and longitudinal susceptibilities $\chi_t(\mathbf{q},\omega)$ and $\chi_l(\mathbf{q},\omega)$ of the C phase depend explicitly on temperature through the Fermi functions of Eq. (34) and vanish as $T\rightarrow 0$. But, as shown in Fig. 12, the normalized integrated intensity

$$\frac{I(\omega)}{n+1}=\frac{1}{n+1}\,(I_i+2s_t)$$
$$=2U^2N(0)\int_{-\infty}^{\infty}d\xi[\mathrm{Im}\chi_t(\xi,\omega)+\mathrm{Im}\chi_l(\xi,\omega)] \tag{43}$$

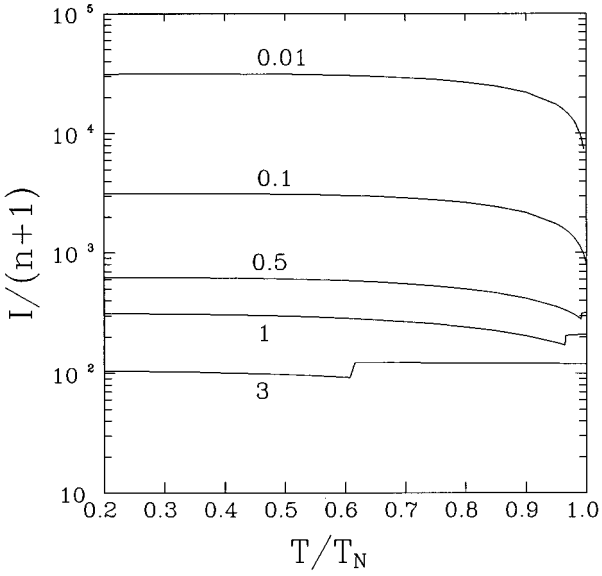

FIG. 12. The total intensity $I=I_i+2s_t$ normalized by $n+1$ vs temperature T/T_N for several values of ω/T_N^* and $z_0/T_N^*=4$.

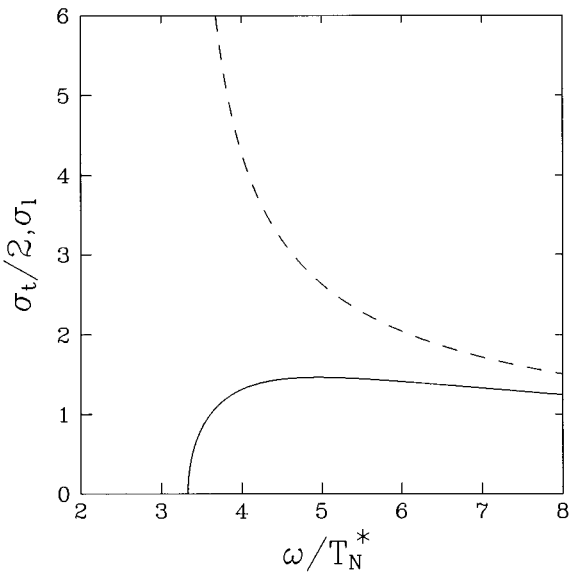

FIG. 13. The transverse (solid) and longitudinal (dash) C cross sections vs ω/T_N^* for $q=0$, $z_0/T_N^*=2$, and $T=0.5T_N$.

is relatively constant. At low temperatures and frequencies, where the SW modes dominate the incoherent background, $I/(n+1)\approx 32\pi\Delta^2/\omega$ depends on temperature primarily through the relatively flat energy gap $\Delta(T)$. So, as in the I phase at low temperatures, the total integrated intensity under the SDW ''chimney'' is approximately proportional to $(n+1)/\omega$. The jump in the $\omega/T_N^*=3$ intensity at $T/T_N=0.64$ occurs as the gap $2\Delta(T)$ drops below ω. For lower frequencies, smaller jumps occur at higher temperatures.

Whereas intraband transitions produce the incoherent background below ω_t, interband transitions across the energy gap produce the background above ω_l. Longitudinal and transverse spin fluctuations cannot be so neatly separated. For a fixed ξ, transverse fluctuations dominate just below ω_t, and longitudinal fluctuations dominate just above ω_l. But intraband transitions below ω_t and interband transitions above ω_l are associated with both longitudinal and transverse spin fluctuations. Nonetheless, longitudinal fluctuations below ω_t and transverse fluctuations above ω_l are disproportionately suppressed as the temperature is lowered.

In Fig. 13, we plot the cross sections $\sigma_t/2$ and σ_l versus frequency for the fixed wave vector $\xi=0$. As expected for this wave vector, both cross sections vanish below the pair-breaking energy 2Δ. At $q=0$, the longitudinal mode corresponds to the vertical transition between the empty circles in Fig. 2(b). As shown in Fig. 13, this enhanced quasiparticle transition is associated with a divergence in the longitudinal susceptibility and a zero in the transverse susceptibility. Whereas the longitudinal cross section decreases monotonically, the transverse cross section reaches a maximum at a frequency of about 3Δ. At very large frequencies $\omega/\Delta\rightarrow\infty$, the spin fluctuations become isotropic with $\sigma_t/2\sigma_l\rightarrow 1^-$. The fluctuations also become isotropic at a fixed frequency as $|\xi|/\omega\rightarrow\infty$.

V. DISCUSSION AND SUMMARY

This paper has developed the RPA for the spin dynamics of itinerant antiferromagnets, and then applied that formalism to the spin dynamics of a CSDW state. Spin excitations with frequency ω and wave vector $p=q+G/2$ about a CSDW with wave vector $G/2$ are associated with quasiparticle transitions with energy change ω and wave-vector change q. The relatively simple quasiparticle energies of the C phase produce a simple spectrum of collective excitations which can be solved analytically using the RPA.

Within the RPA, the C modes do not interact and are undamped. Corrections beyond the RPA would damp the SW and amplitude modes. At nonzero temperatures, anharmonic interactions would generate finite SW lifetimes just as they do in a conventional antiferromagnet. However, because Cr has such a large Néel temperature, the effects of fluctuations on the mode spectrum are expected to be rather small.

The RPA also predicts that the SW modes evolve linearly from each satellite up to arbitrarily high energies. But at the zone center $\mathbf{p}=0$, the SW's evolving from $\mathbf{p}=\pm\mathbf{G}/2$ must meet with zero slope. This discrepancy can be explained by examining the implicit assumptions of our model. As discussed in Appendix B, we assume that the fluctuation energy cq is restricted to a range within $\pm\epsilon_0$ of the Fermi surface. Since the energy cutoff ϵ_0 is much less than the Fermi energy ϵ_F and $k_F<G/2$, the fluctuation momentum q must be much less than $G/2$. So our model is only valid, near the magnetic satellites. In this regime, the cutoff ϵ_0 only enters implicitly through the Néel temperature T_N^* defined by Eq. (B12). A more general model valid near the zone center would involve cutoff-dependent quantities like cq/ϵ_0. Fortunately, the observed spin dynamics of Cr alloys also occurs close to the magnetic satellites.

A high-energy neutron source may be required to test many of the predictions of our model within the C phase. The onset of longitudinal fluctuations at $q=0$ should be observed above the pair-breaking energy of $2\Delta=2\sqrt{2}g$. At low temperatures, $2\Delta(0)=3.52T_N^*\approx 280$ meV is probably too large for detection. But just below the Néel temperature, the order parameter may be small enough to make such an experiment feasible.

The C formalism developed in this paper can also be applied to γ-Mn alloys, which are C itinerant antiferromagnets. But, unlike for Cr alloys, the SW spectrum of γ-Mn alloys contains a gap[19] at zero frequency. The large tetragonal distortion of the fcc γ-Mn lattice may break the rotational symmetry about the spin polarization direction and induce an energy gap in the SW spectrum. The coupling between the SDW and the lattice may be mediated by an associated CDW. We hope to test this conjecture in the near future.

ACKNOWLEDGMENTS

One of us (R.F.) would like acknowledge support from the U.S. Department of Energy under Contract No. DE-FG06-94ER45519. This research was also sponsored by the U.S. Department of Energy under Contract No. DE-ACO5-96OR22464 with Lockheed Martin Energy Research Corporation. S.L. would like to thank Professor L. Sham and Professor R. Dynes for their hospitality at UCSD. Useful conversations with Dr. E. Fawcett, Dr. B. Sternlieb, and Dr. V. S. Viswanath are also gratefully acknowledged.

APPENDIX A

In this appendix, we solve for all quasiparticle transitions subject to the momentum-conservation condition of Eq. (20),

$$z_i(v)-z_j(v-\omega)-\xi=0, \tag{A1}$$

where $\xi=cq$ is the momentum change, and ω is the energy difference. The quasiparticle solutions $\{z_i,v\}$ and $\{z_j,v-\omega\}$ are zeros of the determinant $D(z,\epsilon)$ with band indices i or j. If z_0 is removed by the shift in variables $\epsilon\rightarrow\epsilon+z_0/4$ and $z\rightarrow z+z_0/4$, then the condition $D(z,\epsilon)=0$ can be rewritten as

$$(\epsilon-z)[(\epsilon+z)^2-\kappa^2]=2g^2(\epsilon+z). \tag{A2}$$

As shown in Appendix C, the mismatch energy z_0 only enters the imaginary susceptibilities through the Fermi functions.

In the C regime, the hybridized energies are given by the simple quadratic expression

$$\epsilon^2-z^2=\Delta^2, \tag{A3}$$

where $2\Delta=2\sqrt{2}g$ is the energy gap in Fig. 2(b). Upon squaring Eq. (A1) and using Eq. (A3) to eliminate z^2 terms, we find

$$2v\omega-\omega^2-\xi^2=2z_j\xi. \tag{A4}$$

Squaring this expression and applying Eq. (A3) once more yields

$$v^2-v\omega-\tfrac{1}{4}(\xi^2-\omega^2)-\frac{\xi^2\Delta^2}{\xi^2-\omega^2}=0, \tag{A5}$$

with the two possible solutions

$$v_\pm=\frac{\omega}{2}\pm\frac{\xi}{2}\left(\frac{\xi^2+4\Delta^2-\omega^2}{\xi^2-\omega^2}\right)^{1/2}. \tag{A6}$$

Due to the symmetry of the quasiparticle energies, solutions are always paired with $v_-=\omega-v_+$. Real solutions occur when $\omega^2<\xi^2$ or $\omega^2>\xi^2+4\Delta^2$. The former condition corresponds to transitions within the bottom or top band; the latter condition corresponds to transitions between the two bands.

As expected, the I case is considerably more complicated. Cubing Eq. (A1), using Eq. (A2) to remove the z^3 terms, and then applying Eq. (A1) to eliminate z_j produces

$$\begin{aligned}z_i^2(\omega+3\xi)+z_i[\omega^2-2v(\omega-\xi)-2\xi\omega-3\xi^2]\\ =v^2(3\omega+\xi)+v(-3\omega^2+\xi^2-2\omega\xi)+\omega^3+\omega^2\xi\\ -\omega(\xi^2+\kappa^2+2g^2)-\xi^3+\xi(\kappa^2-2g^2).\end{aligned} \tag{A7}$$

Multiplying by z_i and again applying Eq. (A1) yields

$$\begin{aligned}z_i^2[\omega^2-v(3\omega+\xi)-2\xi\omega-3\xi^2]\\ +z_i[-2v^2(\omega-\xi)+v(3\omega^2-\xi^2+2\omega\xi)-\omega^3-\omega^2\xi\\ +\omega(\xi^2+2\kappa^2)+\xi^3+2\xi(\kappa^2-2g^2)]\\ =-v(v^2-\kappa^2-2g^2)(\omega+3\xi).\end{aligned} \tag{A8}$$

These two relations may be viewed as simultaneous equations for the variables z_i^2 and z_i. Nontrivial solutions are possible when their determinant vanishes. Although the resulting expression is a sixth-order polynomial in v, the sixth- and fifth-order coefficients vanish identically. The remaining expression is quadratic in the variable $x=v(v-\omega)$,

$$ax^2+bx+c=0, \tag{A9}$$

with coefficients

$$a=16(\omega^2-\xi^2)(\omega+\xi)[-(\omega+\xi)^2+4\kappa^2], \tag{A10}$$

$$\begin{aligned}b=8(\omega+\xi)\{2(g^4-2\kappa^4)(\omega^2-\xi^2)-4g^2\kappa^2(\omega^2-5\xi^2)\\ +(\omega+\xi)^2[\kappa^2(\omega-\xi)(5\omega-3\xi)+2g^2\xi(\omega-3\xi)]\\ -(\omega+\xi)^4(\omega-\xi)^2\},\end{aligned} \tag{A11}$$

$$\begin{aligned}c=\{(\omega+\xi)(\omega^2-\xi^2-2g^2)-\kappa^2(\omega-\xi)\}\\ \times\{-4[2\xi g^2-\kappa^2(\omega+\xi)]^2-2g^2(\omega+\xi)^2\\ \times(\omega^2-2\omega\xi+5\xi^2)+\kappa^2(\omega+\xi)^2(5\omega^2-6\omega\xi+5\xi^2)\\ -(\omega+\xi)^4(\omega-\xi)^2\}.\end{aligned} \tag{A12}$$

Equation (A9) guarantees that the I solutions also come in pairs $\{v,\omega-v\}$.

Once the solutions for v are known, Eqs. (A2) and (A3) can be used to find the associated values for z. Only real solutions contribute to the imaginary HF susceptibilities. For a given ω and ξ, there are at most two C or four I real solutions.

APPENDIX B

In this appendix, we derive the zero-frequency real parts $\phi_1^{(i)}(\mathbf{q},0)$ of each HF susceptibility. As shown in Appendix C, the zero-frequency imaginary parts vanish.

We demonstrate the procedure with the fifth HF susceptibility:

$$\begin{aligned}\chi_5^{(0)}(\mathbf{q},0)&=-\frac{T}{V}\sum_{l,\mathbf{k}}G^{\uparrow\uparrow}_{ab+}(\mathbf{k},i\nu_l)G^{\uparrow\uparrow}_{ab+}(\mathbf{k}+\mathbf{q},i\nu_l)\\ &=-\frac{Tg^2}{2}N(0)\sum_l\int dz\,\frac{i\nu_l-z_0/2-\kappa+z}{D(z,i\nu_l)}\\ &\quad\times\frac{i\nu_l-z_0/2-\kappa+z+\xi}{D(z+\xi,i\nu_l)}\\ &\quad+\xi\rightarrow-\xi,\ \kappa\rightarrow-\kappa,\end{aligned} \tag{B1}$$

where Eq. (4) is used for $z(\mathbf{k}+\mathbf{q})$, and $N(0)$ is the single-spin density of states on either the electron or hole Fermi surface (assumed identical). The first set of terms is produced by the $\mathbf{k}$ integral over the northern hemisphere with $k_z>0$; the second set of terms with $\xi\rightarrow-\xi$ and $\kappa\rightarrow-\kappa$ comes from the integration over the southern hemisphere with $k_z<0$.

To evaluate the z integral, we require the imaginary roots of

$$D(z,i\nu_l)=(i\nu_l-z)((i\nu_l-z_0/2+z)^2-\kappa^2)$$
$$-g^2(2i\nu_l-z_0+2z)$$
$$=-(z-z_{1l})(z-z_{2l})(z-z_{3l}). \tag{B2}$$

In the $g\to 0$ limit, $z_{1l}\to i\nu_l$, $z_{2l}\to -i\nu_l+z_0/2-\kappa$, and $z_{3l}\to -i\nu_l+z_0/2+\kappa$. For $g>0$, the roots are defined so that $\mathrm{sgn\,Im}(z_{1l})=\mathrm{sgn}(\nu_l)$ and $\mathrm{sgn\,Im}(z_{2,3l})=-\mathrm{sgn}(\nu_l)$. When $\kappa\to-\kappa$, $z_{2l}\leftrightarrow z_{3l}$. So after completing the contour of the integral in the upper-half-plane for $\nu_l>0$ and the lower-half-plane for $\nu_l<0$, we find

$$\chi_5^{(0)}(\mathbf{q},0)=-\pi iTg^2N(0)\sum_l\left\{\frac{(i\nu_l-z_0/2-\kappa+z_{1l})(i\nu_l-z_0/2-\kappa+z_{1l}+\xi)}{\xi(z_{1l}-z_{2l})(z_{1l}-z_{3l})(z_{1l}-z_{2l}+\xi)(z_{1l}-z_{3l}+\xi)}\right.$$
$$\left.-\frac{(i\nu_l-z_0/2-\kappa+z_{1l}-\xi)(i\nu_l-z_0/2-\kappa+z_{1l})}{\xi(z_{1l}-z_{2l})(z_{1l}-z_{3l})(z_{1l}-z_{2l}-\xi)(z_{1l}-z_{3l}-\xi)}\right\}\mathrm{sgn}(\nu_l)+\xi\to-\xi,\kappa\to-\kappa$$
$$=-4\pi iTg^2N(0)\sum_l Q_l(\xi)\{-(2z_{1l}-z_{2l}-z_{3l})[(i\nu_l-z_0/2+z_{1l})^2+\kappa^2]$$
$$+[(z_{1l}-z_{2l})(z_{1l}-z_{3l})+\xi^2](i\nu_l-z_0/2+z_{1l})\}, \tag{B3}$$

where

$$Q_l(\xi)=\frac{\mathrm{sgn}(\nu_l)}{(z_{1l}-z_{2l})(z_{1l}-z_{3l})[(z_{1l}-z_{2l})^2-\xi^2][(z_{1l}-z_{3l})^2-\xi^2]}. \tag{B4}$$

The $\mathrm{sgn}(\nu_l)$ in the summation over ν_l guarantees that $\chi_5^{(0)}(\mathbf{q},0)=\phi_1^{(5)}(\mathbf{q},0)$ is real.

To simplify our results, we define the variable $i\eta_l=i\nu_l-z_0/2+z_{1l}$. When $|\nu_l|$ is large, $\eta_l\approx 2\nu_l$. Three identities for the roots z_{il} can be obtained by expanding $D(z+\xi,i\nu_l)$ in powers of ξ, and then comparing the coefficients using Eq. (B2):

$$(\eta_1^2+\kappa^2)(i\nu_l-z_{1l})+2i\eta_l g^2=0, \tag{B5}$$

$$(z_{1l}-z_{2l})(z_{1l}-z_{3l})=2g^2-\eta_l^2-\kappa^2-2i\eta_l(i\nu_l-z_{1l}), \tag{B6}$$

$$2z_{1l}-z_{2l}-z_{3l}=-i\nu_l+z_{1l}+2i\eta_l. \tag{B7}$$

The last identity can be also be rewritten as

$$z_{1l}+z_{2l}+z_{3l}=z_0-i\nu_l \tag{B8}$$

for the sum of the three roots.

Using these identities, our results for $\chi_3^{(0)}(\mathbf{q},0)$ through $\chi_6^{(0)}(\mathbf{q},0)$ can be summarized as

$$\phi_1^{(3)}(\mathbf{q},0)=\phi_1^{(4)}(\mathbf{q},0)=-4\pi iTg^2N(0)\sum_l Q_l(\xi)$$
$$\times\{(2z_{1l}-z_{2l}-z_{3l})(\eta_l^2+\kappa^2-\xi^2/2)$$
$$+[(z_{1l}-z_{2l})(z_{1l}-z_{3l})+\xi^2]i\eta_l\}, \tag{B9a}$$

$$\phi_1^{(5)}(\mathbf{q},0)=-4\pi iTg^2N(0)\sum_l Q_l(\xi)$$
$$\times\{(2z_{1l}-z_{2l}-z_{3l})(\eta_l^2-\kappa^2)$$
$$+[(z_{1l}-z_{2l})(z_{1l}-z_{3l})+\xi^2]i\eta_l\}, \tag{B9b}$$

$$\phi_1^{(6)}(\mathbf{q},0)=-4\pi iTg^2N(0)\sum_l Q_l(\xi)$$
$$\times\{(2z_{1l}-z_{2l}-z_{3l})(\eta_l^2+\kappa^2+\kappa\xi)$$
$$+[(z_{1l}-z_{2l})(z_{1l}-z_{3l})+\xi^2]i\eta_l\}, \tag{B9c}$$

which are all real. The identity in Eq. (B9a) follows from the symmetry of the $b\pm$ energies as $\mathbf{k}\to-\mathbf{k}$.

Both $\chi_1^{(0)}(\mathbf{q},0)$ and $\chi_2^{(0)}(\mathbf{q},0)$ are formally divergent. This divergence is removed by using the self-consistent equation for the SDW order parameter,

$$ge^{i\phi_\pm}=-U\frac{T}{V}\sum_{l,\mathbf{k}}G_{ab\pm}^{\uparrow\uparrow}(\mathbf{k},i\nu_l)$$
$$=2\pi ige^{i\phi_\pm}TUN(0)\sum_l\frac{i\eta_l\,\mathrm{sgn}(\nu_l)}{(z_{1l}-z_{2l})(z_{1l}-z_{3l})}, \tag{B10}$$

which can be rewritten as

$$\frac{1}{U}=2\pi iTN(0)\sum_l\frac{i\eta_l\,\mathrm{sgn}(\nu_l)}{(z_{1l}-z_{2l})(z_{1l}-z_{3l})}. \tag{B11}$$

In Eq. (B10), we have temporarily reinstated the phases $\phi_\pm$ to demonstrate how they cancel from the self-consistent equation. The constant Coulomb interaction U can be regarded as the first term in an expansion of $U(\hat{k},\hat{k}')$ in a series[37] of ''kubic harmonics.'' Only the $l=0$, $m=0$ constant term drives the SDW instability of Cr alloys.

When $g=0$ and $z_0=0$, the Matsubara sum in Eq. (B11) can be evaluated by introducing the energy cutoff ϵ_0. If ν_l is summed between $\pm\epsilon_0$, then Eq. (B11) can be written as

$$T_N^* = \frac{2\gamma}{\pi}\,\epsilon_0 e^{-1/UN(0)}, \tag{B12}$$

where T_N^* is the Néel temperature of perfectly nested Cr, and $\ln\gamma \approx 0.577$ is Euler's constant. The cutoff ϵ_0 has precisely the same significance as in BCS theory: quasiparticles are only defined within the range $\pm\epsilon_0$ of the Fermi energy ϵ_F. Although undetermined within BCS theory and within our model of itinerant antiferromagnetism, ϵ_0 is subject to the constraints $T_N^* \ll \epsilon_0 \ll \epsilon_F$.

After separating the formally-divergent contributions from $\phi_1^{(1)}(\mathbf{q},0)$ and $\phi_1^{(2)}(\mathbf{q},0)$, we find

$$\phi_1^{(1)}(\mathbf{q},0) = \phi_1^{(2)}(-\mathbf{q},0) = \frac{1}{U} - 2\pi i TN(0)\sum_l Q_l(\xi)\{(2z_{1l}-z_{2l}-z_{3l})[-2i\eta_l\xi\kappa(i\nu_l - z_{1l}) + \eta_l^2(2g^2+\xi^2+\kappa\xi)$$
$$+ g^2(\xi^2-2\kappa^2) + \xi\kappa^2(\kappa-\xi)] + [(z_{1l}-z_{2l})(z_{1l}-z_{3l}) + \xi^2][i\eta_l(2g^2+\xi^2) + \kappa\xi(i\nu_l - z_{1l})]\}, \tag{B13}$$

where the first equality follows from shifting $\mathbf{k}\to\mathbf{k}-\mathbf{q}$ in the sum of Eq. (16b).

Since all physical results involve the combinations $\chi_{1,2}^{(0)}(\mathbf{q},\omega) - 1/U$, the divergent parts of $\chi_{1,2}^{(0)}(\mathbf{q},0)$ never appear. The self-consistent equation for g is equivalent to the expression

$$\chi_1^{(0)}(0,0) + \chi_3^{(0)}(0,0) - \chi_5^{(0)}(0,0) - \chi_6^{(0)}(0,0) = \frac{1}{U}. \tag{B14}$$

In fact, this identity produces the poles in the transverse and longitudinal susceptibilities at the two SDW satellites.

Specializing to the C regime, $\kappa = 0$ and the roots z_{il} have the analytic solutions

$$z_{1l} = -\tfrac{1}{2}x_l + \frac{z_0}{4}, \tag{B15a}$$

$$z_{2l} = \tfrac{1}{2}\,x_l + \frac{z_0}{4}, \tag{B15b}$$

$$z_{3l} = -i\nu_l + \frac{z_0}{2}, \tag{B15c}$$

$$x_l = -2i\sqrt{\tau_l^2+\Delta^2}\ \mathrm{sgn}(\nu_l), \tag{B16}$$

where $i\tau_l = i\nu_l - z_0/4$, and x_l is defined so that $\mathrm{sgn}\,\mathrm{Im}(x_l) = -\mathrm{sgn}(\nu_l)$. It follows that $i\eta_l = i\nu_l - x_l/2 - z_0/4$,

$$Q_l(\xi) = \frac{-i\ \mathrm{sgn}(\nu_l)}{x_l\eta_l(x_l^2-\xi^2)(\eta_l^2+\xi^2)}, \tag{B17}$$

and that the zero-frequency susceptibilities can be rewritten as

$$\phi_1^{(1)}(\mathbf{q},0) + \phi_1^{(4)}(\mathbf{q},0) = \phi_1^{(2)}(\mathbf{q},0) + \phi_1^{(3)}(\mathbf{q},0)$$
$$= \frac{1}{U} - 2\pi i TN(0)(2\Delta^2+\xi^2)$$
$$\times\sum_l \frac{\mathrm{sgn}(\nu_l)}{x_l(x_l^2-\xi^2)}, \tag{B18a}$$

$$\phi_1^{(5)}(\mathbf{q},0) = \phi_1^{(6)}(\mathbf{q},0) = -2\pi i TN(0)\Delta^2\sum_l \frac{\mathrm{sgn}(\nu_l)}{x_l(x_l^2-\xi^2)}. \tag{B18b}$$

Since the divergent HF susceptibilities always appear in the combinations $\chi_1^{(0)}(\mathbf{q},\omega) + \chi_4^{(0)}(\mathbf{q},\omega)$ and $\chi_2^{(0)}(\mathbf{q},\omega) + \chi_3^{(0)}(\mathbf{q},\omega)$, no further relations are needed.

APPENDIX C

In this appendix, we evaluate the imaginary HF susceptibilities $\phi_2^{(i)}(\mathbf{q},\omega)$, which are defined by analytically continuing the susceptibilities $\chi_i^{(0)}(\mathbf{q},i\omega_n)$,

$$\chi_i^{(0)}(\mathbf{q},\omega+i\varepsilon) = \phi_1^{(i)}(\mathbf{q},\omega) + i\phi_2^{(i)}(\mathbf{q},\omega), \tag{C1}$$

as $\varepsilon\to 0^+$. The formalism used in this section was originally developed for superconductivity by Ambegaokar and Tewordt,[22] and later applied to the C dynamics by Liu.[12]

Each HF susceptibility may be written as a general sum over ν_l:

$$\chi_i^{(0)}(\mathbf{q},i\omega_n) = -T\sum_l P_i(i\nu_l, i\nu_l - i\omega_n;\mathbf{q})$$
$$= T\sum_l \int \frac{d\omega_1}{2\pi}\int \frac{d\omega_2}{2\pi}$$
$$\times \frac{a_i(\omega_1,\omega_2)}{(\omega_1 - i\nu_l)(\omega_2 - i\nu_l + i\omega_n)}, \tag{C2}$$

with the spectral density $a_i(\omega_1,\omega_2)$ defined by

$$a_i(\omega_1,\omega_2) = P_i(\omega_1+i\varepsilon,\omega_2+i\varepsilon) - P_i(\omega_1+i\varepsilon,\omega_2-i\varepsilon)$$
$$- P_i(\omega_1-i\varepsilon,\omega_2+i\varepsilon) + P_i(\omega_1-i\varepsilon,\omega_2-i\varepsilon). \tag{C3}$$

Performing the sum over ν_l then yields

$$\chi_i^{(0)}(\mathbf{q},i\omega_n) = \int \frac{d\omega_1}{2\pi}\int \frac{d\omega_2}{2\pi}\,a_i(\omega_1,\omega_2)\,\frac{f(\omega_1)-f(\omega_2)}{\omega_1-\omega_2-i\omega_n}, \tag{C4}$$

where $f(z) = 1/[\exp(\beta z)+1]$ is the Fermi function. After substituting $i\omega_n\to\omega+i\varepsilon$, we obtain

$$\phi_2^{(i)}(\mathbf{q},\omega) = \tfrac{1}{2}\int \frac{d\omega_1}{2\pi}\,a_i(\omega_1,\omega_1-\omega)[f(\omega_1)-f(\omega_1-\omega)], \tag{C5}$$

which implies that the imaginary susceptibilities vanish when $\omega = 0$.

The spectral density depends on the behavior of the roots z_{il} as $i\nu_l \to \omega + i\varepsilon$. To linear order in ε,

$$z_{il} \to z_i(\omega + i\varepsilon) = z_i(\omega) + \Delta_i , \tag{C6a}$$

$$\Delta_i = i\varepsilon \left(\frac{d\omega}{dz} \right)^{-1} \Bigg|_{z=z_i(\omega)} . \tag{C6b}$$

The real hybridized quasiparticle energies $z_i(\omega)$ are defined so that $dz_1/d\omega \geqslant 0$ and $dz_{2,3}/d\omega \leqslant 0$. When all the solutions are real, $\Delta_1 = i\varepsilon_1$ and $\Delta_{2,3} = -i\varepsilon_{2,3}$, where $\mathrm{sgn}(\varepsilon_i) = \mathrm{sgn}(\varepsilon)$. In the top energy gap, z_1 and z_3 are complex and $\Delta_{1,3}$ contain both real and imaginary parts. Similarly, in the lower-energy gap, z_1 and z_2 are complex, and $\Delta_{1,2}$ contain both real and imaginary parts.

As in Appendix B, we use $\chi_5^{(0)}(\mathbf{q}, i\omega_n)$ to demonstrate the procedure for finding the spectral density:

$$\begin{aligned} \chi_5^{(0)}(\mathbf{q}, i\omega_n) &= -\frac{T}{V} \sum_{l,\mathbf{k}} G^{\uparrow\uparrow}_{ab+}(\mathbf{k}, i\nu_l) G^{\uparrow\uparrow}_{ab+}(\mathbf{k}+\mathbf{q}, i\nu_{l'}) \\ &= -\frac{Tg^2}{2} N(0) \sum_l \int dz \, \frac{(i\nu_l - z_0/2 - \kappa + z)(i\nu_{l'} - z_0/2 - \kappa + z + \xi)}{D(z, i\nu_l)\, D(z+\xi, i\nu_{l'})} + \xi \to -\xi, \kappa \to -\kappa, \end{aligned} \tag{C7}$$

where $\nu_{l'} = \nu_l - \omega_n$. So after completing the contour in the upper-half-plane, we find

$$\begin{aligned} \chi_5^{(0)}(\mathbf{q}, 0) = -\pi i T g^2 N(0) \sum_l \Bigg\{ & \frac{(i\eta_{1l} - \kappa)(i\eta_{1l'} - \kappa + \xi + z_{1l} - z_{1l'})}{(z_{1l} - z_{2l})(z_{1l} - z_{3l})(z_{1l} - z_{1l'} + \xi)(z_{1l} - z_{2l'} + \xi)(z_{1l} - z_{3l'} + \xi)} \, \theta(\nu_l) \\ & + \frac{(i\eta_{1l} - \kappa - \xi + z_{1l'} - z_{1l})(i\eta_{1l'} - \kappa)}{(z_{1l'} - z_{2l'})(z_{1l'} - z_{3l'})(z_{1l'} - z_{1l} - \xi)(z_{1l'} - z_{2l} - \xi)(z_{1l'} - z_{3l} - \xi)} \, \theta(\nu_{l'}) \\ & + \frac{(i\eta_{2l} - \kappa)(i\eta_{2l'} - \kappa + \xi + z_{2l} - z_{2l'})}{(z_{2l} - z_{1l})(z_{2l} - z_{3l})(z_{2l} - z_{1l'} + \xi)(z_{2l} - z_{2l'} + \xi)(z_{2l} - z_{3l'} + \xi)} \, \theta(-\nu_l) \\ & + \frac{(i\eta_{3l} - \kappa)(i\eta_{3l'} - \kappa + \xi + z_{3l} - z_{3l'})}{(z_{3l} - z_{1l})(z_{3l} - z_{2l})(z_{3l} - z_{1l'} + \xi)(z_{3l} - z_{2l'} + \xi)(z_{3l} - z_{3l'} + \xi)} \, \theta(-\nu_l) \\ & + \frac{(i\eta_{2l} - \kappa - \xi + z_{2l'} - z_{2l})(i\eta_{2l'} - \kappa)}{(z_{2l'} - z_{1l'})(z_{2l'} - z_{3l'})(z_{2l'} - z_{1l} - \xi)(z_{2l'} - z_{2l} - \xi)(z_{2l'} - z_{3l} - \xi)} \, \theta(-\nu_{l'}) \\ & + \frac{(i\eta_{3l} - \kappa - \xi + z_{3l'} - z_{3l})(i\eta_{3l'} - \kappa)}{(z_{3l'} - z_{1l'})(z_{3l'} - z_{2l'})(z_{3l'} - z_{1l} - \xi)(z_{3l'} - z_{2l} - \xi)(z_{3l'} - z_{3l} - \xi)} \, \theta(-\nu_{l'}) \Bigg\} + \xi \to -\xi, \kappa \to -\kappa, \end{aligned} \tag{C8}$$

where $\theta(x) = 1$ for $x \geqslant 0$ and 0 otherwise. This defines the function $P_5(i\nu_l, i\nu_{l'})$ from Eq. (C2).

To perform the analytic continuation in Eq. (C3), we use the relation $\theta(\nu_l \to -i\omega + \varepsilon) = \theta(\varepsilon)$. For every possible quasiparticle transition between $z_i = z_i(\omega_1)$ and $\overline{z_I} = z_I(\omega_2)$ with momentum change $-\xi$, the spectral density contains a δ function $\delta(z_i - \overline{z_I} + \xi)$. Because of the sign difference between Δ_1 and $\Delta_{2,3}$, transitions involving z_1 or $\overline{z_1}$ have an extra minus sign. So we find that

$$\begin{aligned} a_5(\omega_1', \omega_2') = -2\pi^2 g^2 N(0) \sum_{i=1}^{3} \sum_{I=1}^{3} & M_i M_I \delta(z_i - \overline{z_I} + \xi) \\ & \times \frac{(\omega_1 + z_i - \kappa)(\omega_2 + \overline{z_I} - \kappa)}{(z_i - z_j)(z_i - z_k)(\overline{z_I} - \overline{z_J})(\overline{z_I} - \overline{z_K})} \\ & + \xi \to -\xi, \kappa \to -\kappa, \end{aligned} \tag{C9}$$

where $M_i = -1$ if $i = 1$ and $+1$ otherwise, $\omega_i' = \omega_i + z_0/4$, and

$$\{i, j, k\} = \{I, J, K\} = \{1, 2, 3\}.$$

Due to the shift in variables ω_i', the roots $z_i(\omega_1)$ and $z_I(\omega_2)$ are evaluated with $z_0 = 0$. When the transition between bands i and I is forbidden, one or both of z_i and $\overline{z_I}$ are complex, and the δ function vanishes.

Although the real parts of $\chi_1^{(0)}(\mathbf{q}, \omega + i\varepsilon)$ and $\chi_2^{(0)}(\mathbf{q}, \omega + i\varepsilon)$ are formally divergent, their spectral densities and imaginary parts are well defined. The spectral densities may be summarized as follows:

$$\begin{aligned} a_i(\omega_1', \omega_2') = -2\pi^2 N(0) \sum_{i=1}^{3} \sum_{I=1}^{3} & M_i M_I \delta(z_i - \overline{z_I} + \xi) \\ & \times \frac{K(\omega_1, z_i, \omega_2, \overline{z_I})}{(z_i - z_j)(z_i - z_k)(\overline{z_I} - \overline{z_J})(\overline{z_I} - \overline{z_K})} \\ & + \xi \to -\xi, \kappa \to -\kappa, \end{aligned} \tag{C10}$$

where

$$K_1+K_4=(\omega_1+z_i-\kappa)(\omega_1+z_i+\kappa)(\omega_2-\overline{z_I})(\omega_2+\overline{z_I}-\kappa), \tag{C11a}$$

$$K_2+K_3=(\omega_2+\overline{z_I}-\kappa)(\omega_2+\overline{z_I}+\kappa)(\omega_1-z_i)(\omega_1+z_i-\kappa), \tag{C11b}$$

$$K_3=g^2(\omega_2+\overline{z_I}-\kappa)(\omega_2+\overline{z_I}+\kappa), \tag{C11c}$$

$$K_4=g^2(\omega_1+z_i-\kappa)(\omega_1+z_i+\kappa), \tag{C11d}$$

$$K_5=g^2(\omega_1+z_i-\kappa)(\omega_2+\overline{z_I}-\kappa). \tag{C11e}$$

$$K_6=g^2(\omega_1+z_i-\kappa)(\omega_2+\overline{z_I}+\kappa). \tag{C11f}$$

The results for $a_1(\omega_1',\omega_2')$ and $a_2(\omega_1',\omega_2')$ have been simplified by combining them with $a_3(\omega_1',\omega_2')$ and $a_4(\omega_1',\omega_2')$.

The imaginary susceptibilities of Eq. (C5) involve integrals of the form

$$\int dv F(v)\delta[z_i(v)-z_I(v-\omega)+\xi]=\left.\frac{F(v)}{|dg_{iI}/dv|}\right|_{v_{iI}}, \tag{C12}$$

where

$$g_{iI}(v,\omega)=z_i(v)-z_I(v-\omega), \tag{C13}$$

and v_{iI} satisfies the momentum-conservation condition $g_{iI}(v_{iI},\omega)=-\xi$. When $z_0=0$, dg_{iI}/dv can be evaluated using the relation for $z_i(v)$,

$$\frac{dz_i}{dv}=\frac{v(v+z_i)^2-\kappa^2 z_i}{z_i(v+z_i)^2-\kappa^2 v}. \tag{C14}$$

Hence the imaginary susceptibilities can be written

$$\begin{aligned}\phi_2^{(i)}(\mathbf{q},\omega)=&-\frac{\pi}{2}N(0)g^2\sum_{v_{iI}}M_iM_I\\&\times[f(\omega_1+z_0/4)-f(\omega_1-\omega+z_0/4)]\frac{1}{|dg_{iI}/d\omega_1|}\\&\times\left.\frac{K(\omega_1,z_i,\omega_1-\omega,\overline{z_I})}{(z_i-z_j)(z_i-z_k)(\overline{z_I}-\overline{z_J})(\overline{z_I}-\overline{z_K})}\right|_{\omega_1=v_{iI}}\\&+\xi\rightarrow-\xi,\kappa\rightarrow-\kappa,\end{aligned} \tag{C15}$$

each of which involves a sum over all possible quasiparticle transitions.

In the C phase, we adopt the following convention for the roots $z_i(v)$:

$$z_1(v)=z_a(v)\equiv\mathrm{sgn}(v)\sqrt{\Delta^2+v^2}, \tag{C16a}$$

$$z_2(v)=\begin{cases}-v, & v>0\\ -z_a(v), & v<0,\end{cases} \tag{C16b}$$

$$z_3(v)=\begin{cases}-z_a(v), & v>0\\ -v, & v<0.\end{cases} \tag{C16c}$$

The C spectral densities can then be written

$$\begin{aligned}&a_1(\omega_1',\omega_2')+a_4(\omega_1',\omega_2')\\&\quad=a_2(\omega_1',\omega_2')+a_3(\omega_1',\omega_2')\\&\quad=\frac{\pi^2N(0)}{2z_a\overline{z_a}}((\omega_1-\omega_2)^2-2\Delta^2-\xi^2)\\&\qquad\times\sum_{m_1=\pm1}\sum_{m_2=\pm1}\delta(m_1z_a+m_2\overline{z_a}+\xi),\end{aligned} \tag{C17a}$$

$$\begin{aligned}&a_5(\omega_1',\omega_2')=a_6(\omega_1',\omega_2')\\&\quad=-\frac{\pi^2\Delta^2N(0)}{2z_a\overline{z_a}}\\&\qquad\times\sum_{m_1=\pm1}\sum_{m_2=\pm1}\delta(m_1z_a+m_2\overline{z_a}+\xi),\end{aligned} \tag{C17b}$$

where $z_a=z_a(\omega_1)$ and $\overline{z_a}=z_a(\omega_2)$.

These spectral densities can be simplified even further using

$$\begin{aligned}\prod_{m_1=\pm1,m_2=\pm1}(m_1z_a+m_2\overline{z_a}+\xi)=&4(\omega^2-\xi^2)(v-v_+)\\&\times(v-v_-),\end{aligned} \tag{C18}$$

where $v_\pm$ are the roots defined in Eq. (A6). So the sum over δ functions can be performed exactly,

$$\begin{aligned}&\sum_{m_1=\pm1}\sum_{m_2=\pm1}\delta(m_1z_a+m_2\overline{z_a}+\xi)\\&\quad=8z_a\overline{z_a}|\xi|\delta\left[\prod_{m_1=\pm1,m_2=\pm1}(m_1z_a+m_2\overline{z_a}+\xi)\right]\\&\quad=2z_a\overline{z_a}|\xi|\delta[(\omega^2-\xi^2)(v-v_+)(v-v_-)].\end{aligned} \tag{C19}$$

Then Eq. (A6) implies

$$\begin{aligned}&a_1(\omega_1',\omega_1'-\omega)+a_4(\omega_1',\omega_1'-\omega)\pm2a_5(\omega_1',\omega_1'-\omega)\\&\quad=-\pi^2N(0)[\theta(\xi^2-\omega^2)+\theta(\omega^2-\xi^2-4\Delta^2)]\\&\qquad\times\left(\frac{\xi^2+4\Delta^2-\omega^2}{\xi^2-\omega^2}\right)^{\pm1/2}\{\delta(\omega_1-v_+)+\delta(\omega_1-v_-)\},\end{aligned} \tag{C20}$$

which is easily transformed into the form of Eq. (34) for the imaginary HF susceptibilities.

APPENDIX D

This appendix summarizes the symmetry relations between the HF susceptibilities. The frequency dependence of each real susceptibility is evaluated from the Kramers-Kronig relation of Eq. (21). After defining the full susceptibility by

$$\chi_i^{(0)}(\mathbf{q},\omega)=\phi_1^{(i)}(\mathbf{q},\omega)+i\phi_2^{(i)}(\mathbf{q},\omega), \tag{D1}$$

and using Eqs. (C11) and (C15) for the imaginary susceptibilities, we find

$$\chi_1^{(0)}(-\mathbf{q},-\omega)=\chi_2^{(0)}(\mathbf{q},\omega)^*, \tag{D2a}$$

$$\chi_3^{(0)}(-\mathbf{q},\omega)=\chi_3^{(0)}(\mathbf{q},\omega), \tag{D2b}$$

$$\chi_4^{(0)}(-\mathbf{q},\omega)=\chi_4^{(0)}(\mathbf{q},\omega), \tag{D2c}$$

$$\chi_3^{(0)}(\mathbf{q},-\omega)=\chi_4^{(0)}(\mathbf{q},\omega)^*, \tag{D2d}$$

$$\chi_4^{(0)}(\mathbf{q},-\omega)=\chi_3^{(0)}(\mathbf{q},\omega)^*, \tag{D2e}$$

$$\chi_5^{(0)}(-\mathbf{q},-\omega)=\chi_5^{(0)}(\mathbf{q},\omega)^*, \tag{D2f}$$

$$\chi_6^{(0)}(\mathbf{q},-\omega)=\chi_6^{(0)}(\mathbf{q},\omega)^*. \tag{D2g}$$

In the C regime,

$$\chi_i^{(0)}(-\mathbf{q},\omega)=\chi_i^{(0)}(\mathbf{q},\omega) \tag{D3}$$

for each correlation function.

APPENDIX E

In this appendix, we demonstrate that the expressions

$$1-U\Psi_{\mp}(\mathbf{q},\omega)=0 \tag{E1}$$

have solutions at the transverse and longitudinal mode frequencies $\omega_t(\mathbf{q})$ and $\omega_l(\mathbf{q})$. Since the imaginary transverse and longitudinal susceptibilities $\Psi_{\mp 2}(\mathbf{q},\omega)$ vanish at ω_t and ω_l, respectively, it remains to show that the real part of Eq. (E1) is satisfied or that

$$U[\Psi_{\mp 1}(\mathbf{q},\omega_{t,l})-\Psi_{\mp 1}(\mathbf{q},0)]$$
$$=1-U\Psi_{\mp 1}(\mathbf{q},0)=2\pi iTUN(0)(2\Delta^2+\xi^2\mp 2\Delta^2)$$
$$\times\sum_l \frac{\mathrm{sgn}(\nu_l)}{x_l(x_l^2-\xi^2)}, \tag{E2}$$

where the right-hand side was evaluated using Eqs. (B15). Now we must evaluate the left-hand side using the Kramers-Kronig relation.

In the transverse case, the left-hand side of Eq. (E2) can be written

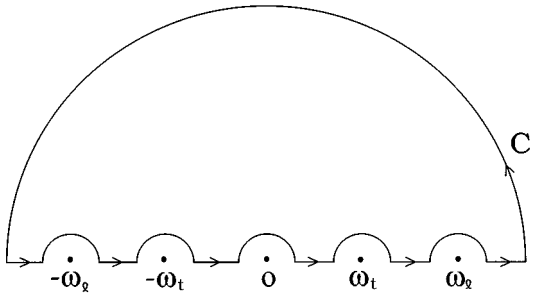

FIG. 14. The contour C used to evaluate the integral J in Appendix E.

$$J_-=\Psi_{-1}(\mathbf{q},|\xi|)-\Psi_{-1}(\mathbf{q},0)$$
$$=\tfrac{1}{2}\,\xi^2N(0)\mathrm{Re}\,P\int_{-\infty}^{\infty}d\omega'\,\frac{1}{\omega'\sqrt{4\Delta^2+\xi^2-\omega'^2}\sqrt{\xi^2-\omega'^2}}$$
$$\times\{f(v'_+ +z_0/4)+f(\omega'-v'_+ +z_0/4)\}, \tag{E3}$$

where $v'_+=v_+(\omega')$. This integral is evaluated on the contour C drawn in Fig. 14. Since the residues at the poles on the real axis all vanish, only the poles in the upper-half-plane contribute to J_-. These poles are produced by the Fermi functions at the points

$$\frac{\omega'}{2}\pm\frac{\xi}{2}\left(\frac{4\Delta^2+\xi^2-\omega'^2}{\xi^2-\omega'^2}\right)^{1/2}=i\nu_l-\frac{z_0}{4}\equiv i\tau_l, \tag{E4}$$

which has four sets of roots given by

$$u_{l\pm}=i\tau_l-d_\pm, \tag{E5a}$$

$$v_{l\pm}=i\tau_l+d_\pm, \tag{E5b}$$

$$d_\pm=\sqrt{-\tau_l^2+\xi^2\pm 2i\xi\tau_l r}, \tag{E6}$$

where $r=ix_l/2\tau_l$, $\mathrm{sgn\,Im}(d_\pm)=\mathrm{sgn}(\nu_l)$, and x_l is defined by Eq. (B16). As $\xi\to 0$, $u_{l\pm}\to 0$ and $v_{l\pm}\to 2i\tau_l$. Notice also that $u_{l+}(-\xi)=u_{l-}(\xi)$ and $v_{l+}(-\xi)=v_{l-}(\xi)$.

Using $\mathrm{sgn\,Im}(v_{l\pm})=\mathrm{sgn}(\nu_l)$ and $\mathrm{sgn\,Im}(u_{l\pm})=-\mathrm{sgn}(\nu_l)$, J_- can be written

$$J_-=2\xi^2N(0)\pi T\ \mathrm{Im}\sum_{l=0}^{\infty}(A_l+B_{-l-1}), \tag{E7}$$

where the residues at $v_{l\pm}$ and $u_{-l-l,\pm}$ are

$$A_l=\frac{2\xi\tau_l(\tau_l+i\xi r-id_-)}{4\tau_l^2(-\tau_l^2-d_-^2)(\tau_l+i\xi r-id_-)^2+4\xi^2\Delta^2(i\tau_l+d_-)^2}+\xi\to-\xi, \tag{E8a}$$

$$B_{-l-1}=\frac{2\xi\tau_l(\tau_l+i\xi r+id_-)}{4\tau_l^2(-\tau_l^2-d_-^2)(\tau_l+i\xi r+id_-)^2+4\xi^2\Delta^2(i\tau_l-d_-)^2}+\xi\to-\xi. \tag{E8b}$$

After some algebra, we find that the sum of residues is given by

$$A_l + B_{-l-1} = \frac{i}{2}\frac{\tau_l r}{\xi(\xi - 2i\tau_l r)}\frac{1}{\tau_l^2+\Delta^2} + \xi \to -\xi$$

$$= \frac{i}{4}\frac{1}{\sqrt{\tau_l^2+\Delta^2}}\frac{1}{\tau_l^2+\Delta^2+\xi^2/4}, \tag{E9}$$

so that

$$J_- = \frac{\xi^2}{2}N(0)\pi T\sum_{l=-\infty}^{\infty}\frac{1}{\sqrt{\tau_l^2+\Delta^2}}\frac{1}{\tau_l^2+\Delta^2+\xi^2/4}$$

$$= 2\pi i TN(0)\xi^2\sum_l \frac{\mathrm{sgn}(\nu_l)}{x_l(x_l^2-\xi^2)}, \tag{E10}$$

which is the desired result.

The longitudinal case is very similar. In Eq. (E3), the prefactor $\omega_t^2=\xi^2$ must be replaced by $\omega_l^2=\xi^2+4\Delta^2$. Otherwise, J_+ is identical to J_-, and the steps described above produce

$$J_+ = 2\pi i TN(0)(\xi^2+4\Delta^2)\sum_l \frac{\mathrm{sgn}(\nu_l)}{x_l(x_l^2-\xi^2)}, \tag{E11}$$

in agreement with Eq. (E2).

*Current address.

[1] For comprehensive reviews of Cr alloys, see E. Fawcett, Rev. Mod. Phys. **60**, 209 (1988); E. Fawcett, H. L. Alberts, V. Yu. Galkin, D. R. Noakes, and J. V. Yakhmi, *ibid*. **66**, 26 (1994).

[2] S. K. Sinha, S. H. Liu, L. D. Muhlestein, and N. Wakabayashi, Phys. Rev. Lett. **23**, 311 (1969).

[3] J. Als-Nielsen, J. D. Axe, and G. Shirane, J. Appl. Phys. **42**, 1666 (1971).

[4] S. K. Sinha, G. R. Kline, C. Stassis, N. Chesser, and N. Wakabayashi, Phys. Rev. B **15**, 1415 (1977).

[5] K. Mikke and J. Jankowska, in *Proceedings of the Conference on Transition Metals*, Toronto, 1977, edited by M. J. G. Lee, J. M. Pirz, and E. Fawcett, IOP Conf. Proc. No. 39 (Institute of Physics and Physical Society, London, 1978), p. 599; J. Phys. F **10**, L159 (1980).

[6] C. R. Fincher, Jr., G. Shirane, and S. A. Werner, Phys. Rev. Lett. **43**, 1441 (1979).

[7] C. R. Fincher, G. Shirane, and S. A. Werner, Phys. Rev. B **24**, 1312 (1981); S. A. Werner, G. Shirane, C. R. Fincher, and B. H. Grier, in *Neutron Scattering—1981*, edited by John Faber, Jr. (AIP, New York, 1982), p. 269; B. H. Grier, G. Shirane, and S. A. Werner, Phys. Rev. B **31**, 2892 (1985).

[8] S. K. Burke, W. G. Stirling, K. R. A. Ziebeck, and J. G. Booth, Phys. Rev. Lett. **51**, 494 (1983).

[9] J. E. Lorenzo, B. J. Sternlieb, G. Shirane, and S. A. Werner, Phys. Rev. Lett. **72**, 1762 (1994).

[10] Y. Endoh, T. Fukuda, K. Yamada, and M. Takeda, J. Phys. Soc. Jpn. **63**, 3572 (1994).

[11] P. A. Fedders and P. C. Martin, Phys. Rev. **143**, 8245 (1966).

[12] S. H. Liu, Phys. Rev. B **2**, 2664 (1970).

[13] M. B. Walker, Can. J. Phys. **54**, 1240 (1976).

[14] R. S. Fishman and S. H. Liu, following paper, Phys. Rev. B **54**, 7252 (1996).

[15] R. S. Fishman and S. H. Liu, Phys. Rev. B **48**, 3820 (1993).

[16] C. Y. Young and J. B. Sokoloff, J. Phys. F **4**, 1304 (1974).

[17] R. S. Fishman and S. H. Liu, Phys. Rev. B **50**, 4240 (1994).

[18] In Ref. 17, we mistakenly concluded that the *C* longitudinal mode *was* associated with a δ function.

[19] M. C. K. Wiltshire, M. M. Elcombe, and C. J. Howard, J. Phys. F **15**, 1595 (1985).

[20] X. W. Jiang and R. S. Fishman (unpublished).

[21] M. A. Lind and J. L. Stanford, Phys. Lett. **39A**, 5 (1972).

[22] V. Ambegaokar and L. Tewordt, Physiol. Rev. **134**, A805 (1964).

[23] H. A. Mook, J. W. Lynn, and R. M. Nicklow, Phys. Rev. Lett. **30**, 556 (1973); H. A. Mook and D. McK. Paul, *ibid.* **54**, 227 (1985).

[24] H. Sato and K. Maki, Int. J. Magn. **4**, 163 (1973). : **6**, 183 (1974).

[25] Yu. A. Izyumov andV. M. Laptev, Zh. Eksp. Teor. Fiz. **88**, 165 (1985) [Sov. Phys.-JETP **61**, 95 (1985)].

[26] T. Ziman and P. Lindgård, Phys. Rev. B **33**, 1976 (1986).

[27] X. Zhu and M. B. Walker, , Phys. Rev. B **34**, 8064 (1986).

[28] S. H. Liu, , Phys. Rev. B **13**, 3962 (1976); J. Magn. Magn. Mater. **25**, 97 (1981).

[29] A. B. Harris, D. Kumar, B. I. Halperin, and P. C. Hohenberg, Phys. Rev. B **3**, 961 (1971).

[30] J. B. Sokoloff, Phys. Rev. **185**, 770 (1969); **185**, 783 (1969).

[31] G. C. Psaltakis, Solid State Commun. **51**, 535 (1984).

[32] P. B. Littlewood and C. M. Varma, Phys. Rev. B **26**, 4883 (1982).

[33] A. F. Volkov and Sh. M. Kogan, Zh. Eksp. Teor. Fiz. **65**, 2038 (1973) [Sov. Phys. JETP **38**, 1018 (1974)].

[34] R. S. Fishman and S. H. Liu, Phys. Rev. B **47**, 11 870 (1993); J. Phys. C **5**, 3959 (1993).

[35] E. Fawcett, S. A. Werner, A. Goldman, and G. Shirane, Phys. Rev. Lett. **61**, 558 (1988).

[36] D. R. Noakes, T. M. Holden, E. Fawcett, and P. C. deCamargo, Phys. Rev. Lett. **65**, 369 (1990).

[37] F. C. Von der Lage and H. A. Bethe, Phys. Rev. **71**, 612 (1947).